ADAPTATION STRATEGIES TO MITIGATE IMPACTS OF SEA LEVEL RISE ON A FRESHWATER AQUIFER SUPPLY ON A BARRIER ISLAND

A Thesis

Submitted to the Graduate Faculty of the
University of South Alabama
in partial fulfillment of the
requirements for the degree of

Master of Science

in

Civil Engineering

by
Kaylyn C. Bellais
B.S., University of South Alabama, 2018
May 2022

ACKNOWLEDGEMENTS

All glory be to God the Father, the Son, and the Holy Spirit for all the abilities that went into this thesis. This thesis work was a result of the community meetings with Dauphin Island; without their input, this project would not have existed. I thank all my family and my friends for their support along the way. I also thank Dr. Stephanie Patch, Dr. Bret Webb, and Dr. Kari Lippert. A special thank you to Renee Collini, Mikaela Heming, and Carey Shaefer from Mississippi State Coastal Extension Center, Peyton Caraway, Benji Delaney, and Dauphin Island stakeholders: residents, state, and federal officials.

TABLE OF CONTENTS

Page

LIST OF TABLES

LIST OF FIGURES

Figure Page

LIST OF ABBREVIATIONS

SLR	=	Sea-Level Rise
SEAWAT	=	coupling software used for 3D groundwater transport of nonuniform density
ATPs	=	Adaptation Tipping Points
APs	=	Adaptation Pathways
AL	=	Alabama
UTM	=	Universal Transverse Mercator
MSL	=	Mean Sea Level
FEMA	=	Federal Emergency Management Agency
DEM	=	Digital Elevation Model
LiDAR	=	Light Detection and Ranging
d	=	Depth
NOAA	=	National Oceanic and Atmospheric Administration
NAVD88	=	North American Vertical Datum of 1988
GMSL	=	Global Mean Sea Level
MSL	=	Mean Sea Level

ABSTRACT

Bellais, Kaylyn, C., M. S., University of South Alabama, May 2022. Adaptation Strategies to Mitigate Impact of Sea Level Rise on a Freshwater Aquifer Supply on a Barrier Island. Chair of Committee: Stephanie Patch, Ph.D., P.E.

Adaptation strategies are used to reduce vulnerability in response to storms and sea-level rise (SLR). An adaptation tipping point for a barrier island is said to exist when an adaptation strategy fails. Previous studies have applied statistics to identify adaptation tipping points and construct adaptation pathways as a function of quantity of SLR. This study is focused on Alligator Lake and Oleander Pond on the barrier island Dauphin Island, AL; a site residents and community leaders identified as vulnerable to saltwater intrusion under future SLR conditions. Therefore, the purposes of this study are to numerically simulate impacts of a storm and SLR scenarios on a barrier island freshwater aquifer, evaluate the effectiveness of adaptation strategies to prevent seawater contamination via overtopping as sea levels rise, and develop an adaptation pathway for protecting the freshwater supply under future climate scenarios. XBeach was used to simulate morphological changes to the region near Alligator Lake and Oleander Pond with merged DEM and Lidar data. SLR scenarios (0.40 m, 0.53 m, 0.66 m, 0.75 m, 1.00 m, 1.26 m, and 1.93 m) were simulated with Hurricane Nate hydrodynamic conditions. Overtopping occurred at 1.26 m and 1.93 m of SLR. An adaptation pathway was created with four adaptation strategies and seven SLR scenarios.

CHAPTER I

INTRODUCTION

This thesis will review barrier island response to sea-level rise, hydrodynamic processes, saltwater intrusion of coastal aquifers, adaptation strategies, and adaptation tipping points. The study site will be introduced describing geographical features, Hurricane Nate storm conditions, and current adaptation strategies. A methodology will describe the model, grids, and plots used to simulate tides and total water levels. The results will include initial, peak, and final water levels, dune crest elevations, and initial, final, and change in bathymetry. The effectiveness of the adaptation strategies will be discussed by comparing the adaptation strategies to one another and previous work. An adaptation pathway will be developed from comparisons. This thesis will conclude with the main findings (water levels and dune crest elevations), adaptation strategy effectiveness, and construction of the adaptation pathway.

1.1 Barrier Island response to sea-level rise

Sea-level rise (SLR) is primarily driven by ocean thermal expansion and input from melting land glaciers and terrestrial water bodies (IPCC, 2007). SLR disrupts tidal ranges, current velocities, and circulation (French, 2008; Hall et al., 2013; Leorri et al., 2011; Valentim et al., 2013). Rapid rates of SLR cause coastal environments such as barrier islands to transition from shoreline retreat to flooding (Donoghue, 2011). The duration of the transition period is determined by sediment supply and subsidence. Moore

et al. (2010) suggest that because of SLR or reduced sediment accretion, barrier islands move onshore, disintegrate during storms because of sediment deficiency and lack of higher elevations, or submerge to become marine sedimentary features. If SLR is absent, a barrier island does not exist because the back barrier fills with sediment transported by a connecting water body (e.g. river) (Beets and van der Spek, 2000; Nienhuis & Lorenzo-Trueba, 2019). Moderate SLR allows marsh and tidal flats to exist on the backside of the island, and island stability is achieved by onshore migration which occurs during storms and tides bringing in cross-shore deposits from the seaward side. No SLR and moderate SLR do not impact the back barrier in the same way because the sediment discharge from a river would differ due to time and sediment volume compared to overwashed sediment brought in by a storm from the seaside. Higher SLR is a hazard to barrier islands since less area exists above the water surface (Nienhuis and Lorenzo-Trueba, 2019). If sediment supply fails to properly supply barrier islands, the island will drown in place (Mellet and Plater, 2018; Rodriguez et al., 2001). Barrier islands that do not adjust to SLR may submerge because of lower bed elevations or reduce in island width because of shoreline retreat and narrowing (Ciarletta et al., 2019; Lorenzo-Trueba & Ashton, 2014; Miselis & Lorenzo-Trueba, 2017).

1.2 Hydrodynamic and morphodynamic processes

Storm occurrence determines barrier island stability with respect to SLR (Houser & Hamilton, 2009). Duran and More (2013) suggest that areas with large established dune systems are at risk for major deformation and irreversible equilibrium states because

they rely on beach and vegetation recovery. The foredune serves as the major line of defense for a barrier island, and its ability to protect is limited to excursion (tides + storm surge + wave runup) (Houser and Hamilton, 2009; Morton, 2002; Nott, 2006; Sallenger, 2000; Thieler and Young, 1991). Wave runup is the vertical distance waves reach on the beach (Bertin et al., 2018) driven by setup or swash (Stockdon et al., 2006). When excursion is greater on the seaward side versus the back barrier side of the island, storm overwash carries sediment to the back barrier side (Carruthers et al., 2013; Donnelly et al., 2006). Runup overwash results during high tides leaving small tapering deposits, and inundation overwash results from barrier submergence leaving cross-shore deposits 100-1000 m wide (Donnelly, 2006; Sallenger, 2000). Overwash events collectively cause landward expansion which creates conditions necessary for barrier islands to sustain SLR over geologic time (Leatherman, 1983). Long-term overwash events are not well bounded, and their connection to current overwash events is unclear (Carruthers et al., 2013; Donnelly et al., 2006; Lazarus, 2016; Rodgers et al., 2015). Unconfined long-term overwash events have yielded barrier island overwash models that depend on geometry and rollover rather than individual storms.

1.3 Saltwater intrusion of coastal aquifers

Breached coastal areas, inundation, and saltwater intrusion of coastal aquifers occur as successive events (Elsayed, 2017). Breaching facilitates onshore flooding by allowing seawater to transport through channels toward land. Transported seawater could then potentially seep down into groundwater (Yang et al., 2013). However, breaching and

flooding occur within days while saltwater intrusion may occur over several years. Breaching is driven by immense overtopping (Kanning et al., 2007; Vorogushyn et al., 2009). Chang et al. (2011) proposed that SLR would induce pressure on the seaside of an aquifer causing the water table elevation to rise. SLR impacts on coastal aquifers were observed by analyzing the position of a salt wedge in a confined and unconfined aquifer. Numerical outputs from SEAWAT, a coupling software used for 3D groundwater transport of nonuniform density (Guo and Bennett, 1998), showed that a steady-state salt wedge in a confined aquifer will be unaffected by SLR for constant, continuous recharge. In a shortened simulation, the salt wedge position for the confined aquifer initially contaminated the aquifer but did return to its original location. The salt wedge position for an unconfined aquifer did not return to its original location since water is able to flow at deeper depths within the aquifer. Although the salt wedge positions differed for the confined and unconfined aquifer, model outputs showed that SLR elevated both aquifers and that upward forcing can reduce long-term saltwater intrusion affects. Remediation strategies to coastal breaching, flooding, and saltwater intrusion of coastal aquifers include budgeting for coastal aquifer pollution in flood risk, designing drainage systems that account for overtopping, and managing susceptible areas without the use of open channels and open wells since they would facilitate contamination (Elsayed, 2017).

1.4 Adaptation strategies

An adaptation strategy to SLR and the resulting saltwater intrusion may individually incorporate or combine planned retreat, accommodation, and protection

(Bijlsma et al., 1996). Examples of planned retreat, accommodation, and protection include acquiring land, increasing the height of houses, and beach nourishment (Doberstein et al., 2019 adapted from Tyler, 2015). An effective adaptation strategy uses multiple adaptation approaches which are customized to meet the requirements of a vulnerable area and attempt to lessen implementation constraints (Klein et al., 1999). Adaptation strategies are also characterized according to reactive or anticipatory adaptation (Burton, 1997; Klein and Tol, 1997; Smit, 1993; Smit et al., 1999). Reactive adaptation follows climate change conditions, and anticipatory adaptation precedes climate change conditions. However, reactive and anticipatory adaptation are sometimes indistinct from the other, especially in a persistent, evolving system. Adaptation can be autonomous or planned. Autonomous adaptation occurs in the absence of a decision-maker, and planned adaptation operates under carefully organized instruction. Although natural systems respond with reactive and autonomous adaptation, planned and anticipatory adaptation may enhance autonomous adaptation such as making area available for planned retreat or beach nourishment.

1.5 Adaptation tipping points

Adaptation tipping points (ATPs) are instances when management strategies can no longer fulfill their intended outcomes because of changing environmental factors (Kwadijk et al., 2010). Adaptive policies should account for time and a system's response to current change to gauge future conditions and conditions leading up to the future (Yohe, 1990). The ATP approach incorporates time (Walker et al., 2013) and considers

the circumstances that cause a plan to reach its threshold rather than trying to anticipate a climate scenario (Kwadijk et al., 2010). ATPs exist within the ATP approach, which focuses on planning for the implementation of adaptation strategies; thus an ATP indicates when a new adaptation strategy is needed within the approach. Adaptation pathways (APs) are selected avenues that provide outcomes for a system susceptible to climate change and use gradual tiers activated when a shift in circumstances occurs (Haasnoot et al., 2013; Kwadijk et al., 2010; Parson & Karwat, 2011; Ranger et al., 2013; Walker et al., 2013; Wise et al., 2014). Therefore, APs are activated by ATPs (Kwadijk et al., 2010; Ranger et al., 2013; Walker et al., 2013; Wise et al., 2014). The AP approach is time based (Walker et al., 2013) and branches from the ATP approach by using alternate plans when a tipping point occurs (Figure 1) (Haasnoot et al., 2011; Haasnoot et al., 2012).

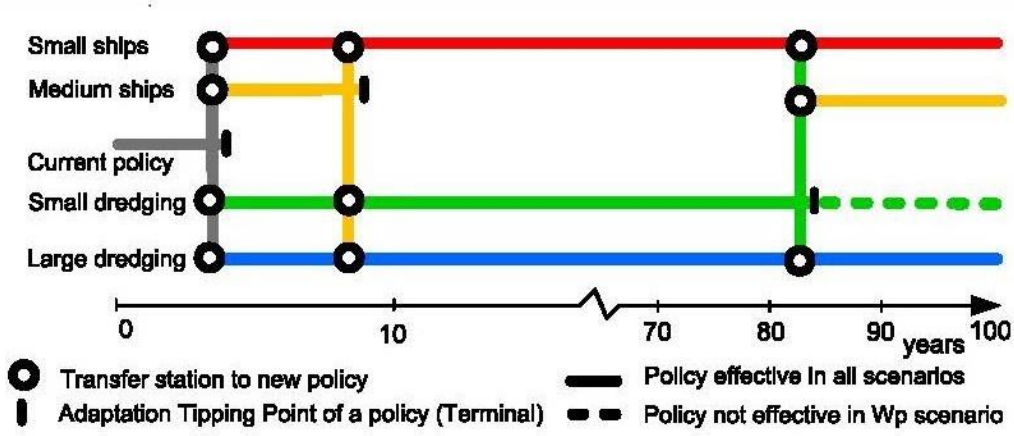

Figure 1. An adaptation pathway was created for low flow management showing adaptation strategies with respect to time (Haasnoot et al., 2012).

Ramm et al. (2018) previously constructed an AP for Lakes Entrance, Australia with adaptation strategies being a function of use-by year, which is the predicted time that an ATP will take place (Haasnoot, et al., 2015), and ATPs being associated with SLR magnitudes. ATPs were determined from scenario discovery which uses a statistical approach. However, we explore adaptation strategies as a function of SLR magnitude using XBeach similar to Smallegan et al. (2017) who develop an AP for Bay Head, New Jersey. The AP itself is an indicator of time because the amount of SLR, which determines when an adaptation strategy should be put into place, is inherently dependent on water level increases over time.

1.6 Study purpose

The purpose of this study is to determine the vulnerability of a freshwater aquifer to overtopping and overwashing as sea levels rise by (1) exploring Hurricane Nate and SLR impacts at Dauphin Island, Alabama near Alligator Lake and Oleander Pond (aquifer site) through numerical modelling (Xbeach), (2) simulating adaptation strategies to increase the resilience of the aquifer to SLR impacts, and (3) developing an adaptation pathway in response to simulated adaptation strategies. The background and study site will follow in Chapter II.

CHAPTER II

BACKGROUND AND STUDY SITE

2.1 Geomorphology

Dauphin Island is a barrier island with an area of 16 km^2 (3,954 acres) (Ellis et al., 2018) and is located off the coast of Mobile County, Alabama (AL) with universal transverse mercator (UTM) coordinates 16 R 392981 m E 3347483 m N (Figure 2) (Google Earth Pro, 2022). Geologic events reveal the island's formation/transformation over time and can be used to assess present-day island vulnerability/resilience. Geometry of the east end is attributed to Pleistocene erosion and uplifting and Holocene strand plains (Otvos, 1970). Island thinning on the west end is driven by longshore current and overwash (Otvos, 1970; Riggs et al., 1995). Core samples collected from Cedar Key and Little Dauphin Island (connected to the east end of Dauphin Island) reveal normal grading (coarse to fine sediment) indicating washover (Ellis et al., 2018). Sediment between Graveline Bay (located on the back barrier side of the east end of Dauphin Island between Lafitte Bay and Bayou Aloe) and Dauphin Island suggest variable influences from storms and human impacts. Ellis et al. (2018) do not state which human impacts direct sediment transport in the cross-shore direction, but perhaps there are lack of data that point to a specific event(s). Estuarine sediment in marshes may also result from wave propagation in the Mississippi Sound during storms. Present-day sediment transport, driven by southeast wind and waves, primarily occurs in the longshore direction from east to west (Byrnes et al., 2013). The east end experiences longshore transport reversals, but the reversals do not largely influence overall transport.

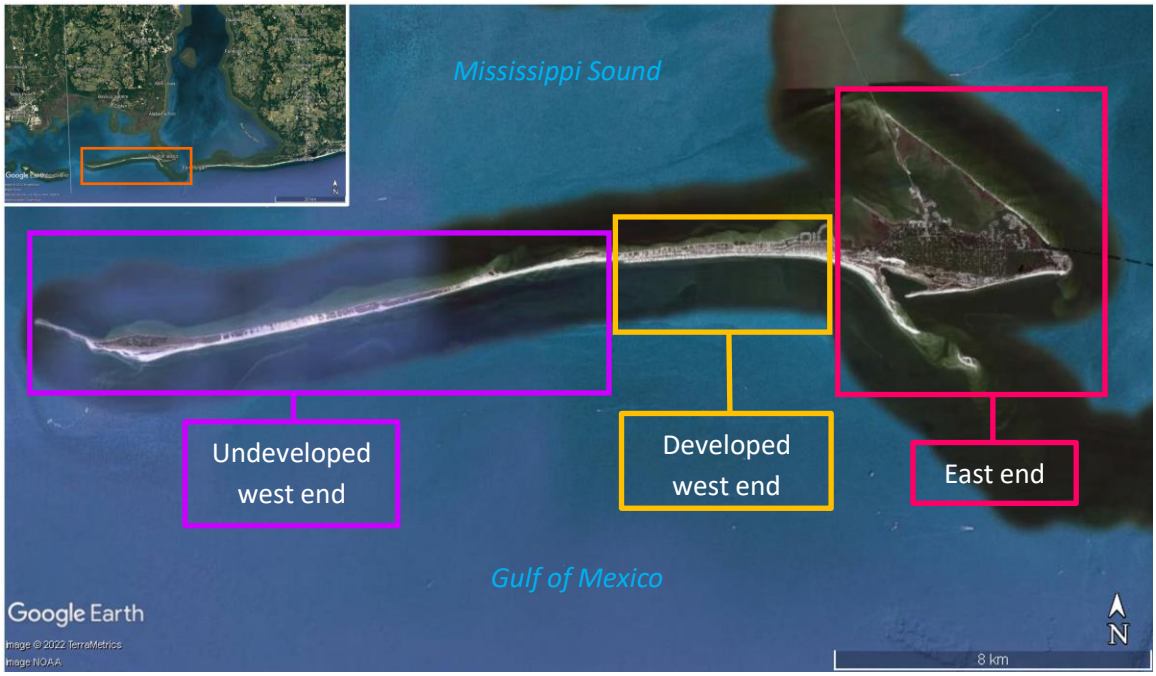

Figure 2. Dauphin Island is located off the coast of Mobile County, AL (orange box) (Google Earth Pro, 2022). The undeveloped west end (purple box) is the western most part, the developed west end (gold box) is the central part of the island, and the east end (pink box) is the eastern most part.

2.2 Wind, waves, and water levels

Dauphin Island has a south facing beach, and winds typically blow out of the southeast (USACE-ERDC, 2014a) driving waves toward shore in the north to northwest direction (USACE-ERDC, 2014b). Tides at Dauphin Island are diurnal with winter months experiencing lower tides than summer months due to tides following mean sea level (MSL). To illustrate this, according to the average seasonal cycle from Dauphin Island tide gauge 8735180, MSL is -0.113 in January while MSL is 0.132 in September (Figure 3) (NOAA-TC, 2022a). The current rate of relative sea level rise at Dauphin Island is 4.13 +/- 0.59 mm/yr (NOAA-TC, 2021). Measured wind, wave, tides, storm

surge, and SLR parameters are of interest because they will be used as inputs in coastal numerical models as discussed later in this document.

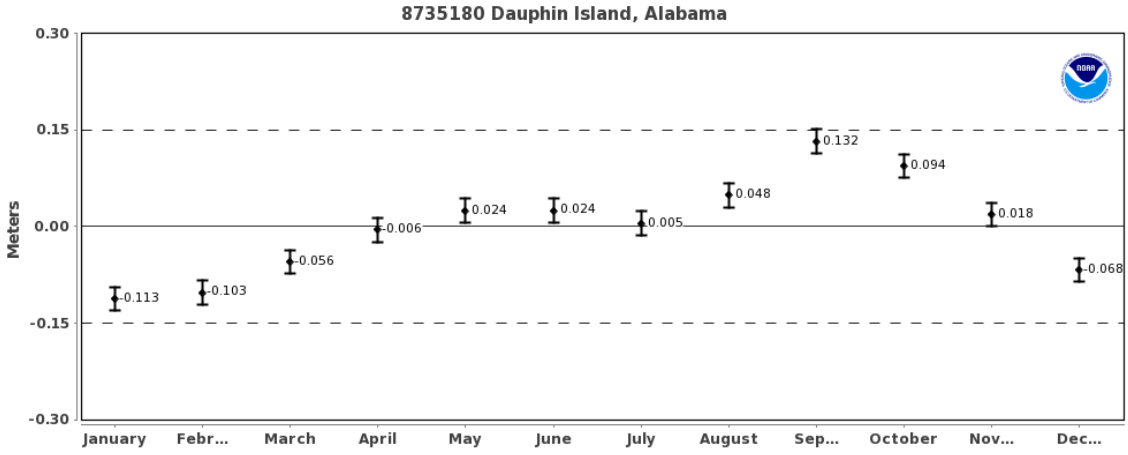

Figure 3. The average seasonal cycle shows MSL from Dauphin Island tide gauge 8735180 (NOAA – TC, 2022a).

2.3 Dauphin Island aquifers

Kidd (1988) recognizes the deep sand (bottom aquifer), the shallow sand (middle aquifer), and the water-table (top aquifer) as freshwater aquifers for Dauphin Island, AL (Figure 4). The deep sand aquifer is Miocene age and extends 152 m below sea-level (Chandler and Moore, 1983). The lower portion of the shallow sand aquifer is Miocene age and extends 46 – 152 m below sea-level while the upper portion of the shallow sand aquifer is Pleistocene age and extends 15 – 46 m. The shallow sand aquifer is overlain by 9 m of clay (O'Donnell, 2005). The water-table aquifer includes the Gulfport Formation of Otvos (Pleistocene age) and is overlain by Holocene sand (Luttrell et al., 1981). The water-table aquifer has a depth of approximately 13 m (O'Donnell, 2005). Elevated

chloride levels in the deep sand aquifer make it unsuitable for human consumption. Therefore, the shallow sand and water-table aquifers provide the most readily available freshwater (Petty, 2011). The aquifers are supplied by a freshwater lens that overlies saltwater because of lower density, water-table elevation, low permeability layers, and slow spreading with saltwater. The lens is supplied by precipitation.

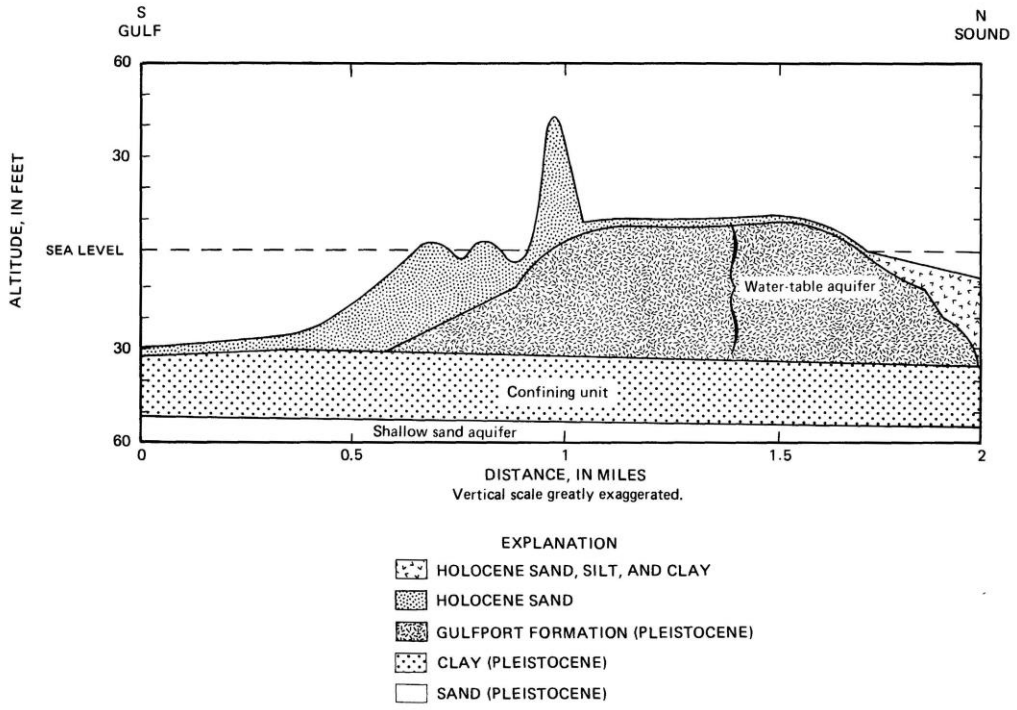

Figure 4. A generalized south-north hydrologic section of Dauphin Island is shown (modified from Otvos, 1985) (Kidd, 1988). Note that the deep sand aquifer is not depicted.

2.4 Historic storm impacts

Hurricanes Frederic, Ivan, and Katrina have greatly altered Dauphin Island through breaching, overwash, erosion, and rollover (Steyer et al., 2020). Specifically, Frederic resulted in washover deposits on the west end while the east end incurred minor damage because of a sizeable dune system fronting it (Halper and Schroeder, 1990; Parker et al., 1981). Ivan created channels at the west end, and Katrina widened a channel also the west end (undeveloped section) (Froede, 2008; Winstanley, 2013). Pelican-Sand Island protected the east end of Dauphin Island during Ivan at the expense of near total dune erosion (Winstanley, 2013). Katrina eroded dunes and beach at the undeveloped section on the west end while the east end experienced minor impacts (Froede, 2008). Pelican-Sand Island also migrated to the northwest. Pre- Ivan and Katrina breaches have recovered over decades because of sediment transport from Mobile Pass ebb-tidal delta (Byrnes et al., 2010; Morton, 2008). Katrina Cut (the largest breach) was filled during the summer of 2010 to the spring of 2011 with a sand-tight rubble mound structure (Webb et al., 2011). During Hurricane Nate (October 8, 2017) at 3:50 a.m., wind speeds reached 16.2 m/s producing 5 m wave heights according to station 42012 at water depth of 25.9 m (NOAA-NDBC, 2017) (Figure 5). Tides and storm surge at 3:48 a.m. were 1.014 m and 0.724 m (NAVD88) according to the Dauphin Island tide gauge 8735180 (NOAA-TC, 2017).

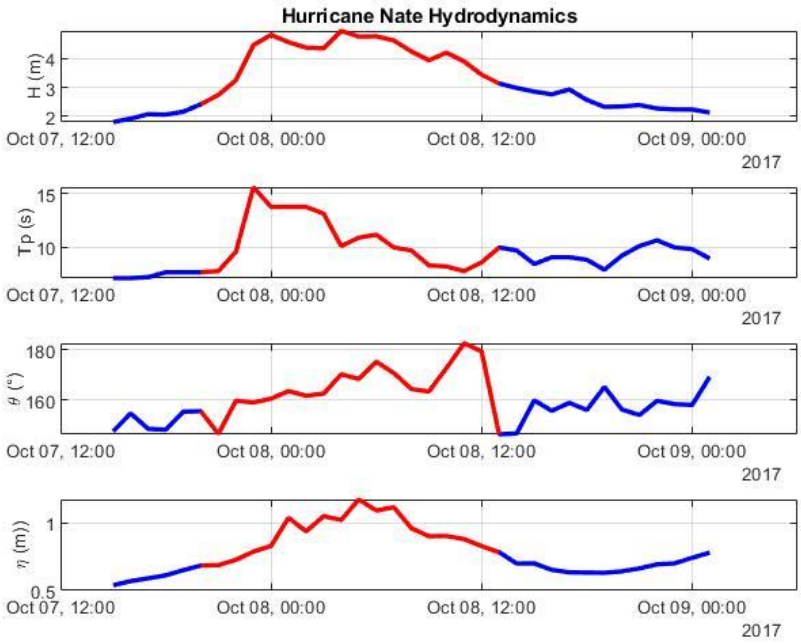

Figure 5. Wave height (H), peak wave period (T_p), and wave direction (θ) were measured from NOAA data buoy station 42012, and excursion (η) was measured from Dauphin Island tide gauge 8735180 during Hurricane Nate. The red line was the extent of the storm in which morphodynamic change was observed on the west end while the blue line was the duration of the complete the storm.

2.5 Armoring, sediment transport, and nourishment strategies

Previous strategies for Dauphin Island include armoring Fort Gaines with riprap on the east end, placing groins on the southeast end, installing retaining walls on the northeast end, placing riprap at the western fishing pier, and building berms on the west end in response to Hurricane Georges, Tropical Storm Isadore, and Hurricanes Ivan and Katrina (Steyer et al., 2020). Emergency berms were built on the west end in 2007 as an attempt to armor homes facing the Gulf side (Froede, 2010). However, the berms over-steeped the shoreline and were eroded by Hurricane Gustav in 2008, and Federal Emergency Management Agency (FEMA) forwent funding because of the lack of homes

in the area. During the 2010 Deepwater Horizon oil spill, riprap was placed at the Katrina breach to avert oil from the Mississippi Sound. The riprap was subject to be removed by summer of 2011 per an emergency permit, but a permanent permit was also applied for during the time of construction to allow the structure to remain in place (Webb et al., 2011). Newer strategies for the east end of Dauphin Island have included converting groins to breakwaters and constructing a pocket beach.

2.6 Proposed nourishment and land acquisition strategies

The Alabama Barrier Island Restoration Assessment Monitoring and Adaptive Management plan includes ebb tidal shoal, gulf beach, back barrier and marsh restoration, and land acquisition as ecosystem restoration measure types for Dauphin Island (Steyer et al., 2020). The ebb tidal shoal restoration measure type aims to attenuate wave impacts on the east end, nourish the beach and tidal flat, and mitigate land loss using 3.4 million cubic meters (4.4 million cubic yards) of sand southeast of Pelican Island for longshore sediment transport. The ebb tidal shoal restoration measure type also intends to nourish and build Sand Island and Pelican shoal systems with 3.3 million cubic meters (4.3 million cubic yards) of sand. The gulf beach restoration measure type focuses are nourishing beaches and building dunes for the east end, west end, and Katrina Cut and deconstructing the Katrina Cut structure. The east end will use 917,466 cubic meters (1.2 million cubic yards) of sand for the beach and dunes, and fencing will be placed along with flora for the dunes. Six million cubic meters (7.8 million cubic yards) of sand, flora, and fencing will be used for the west end, Katrina Cut, and dune restoration after

225 houses are purchased based on homeowners willing to sell their homes. The back barrier and marsh restoration measure type intends to rebuild intertidal and back barrier flat habitat, expand back barrier meadow and wetland habitats, and aid marsh response to SLR by nourishing 31 of the 2010 inactive borrow pits with 214,458 cubic meters (280,500 cubic yards) of fill. Implementation of living shorelines is also proposed to help with marsh restoration. Various acreage throughout Dauphin Island is desired to reduce development impacts to the island. Currently (winter of 2022), the east end is in the stakeholder engagement and design phase, and construction is expected to take place by summer of 2023 (Town of Dauphin Island, 2022a). The project for the west end has not begun, but investigations and stakeholder engagement will begin by summer of 2022 (Town of Dauphin Island, 2022b).

2.7 Study site

Alligator Lake (16R 395344 m E 3346671 m N) has an estimated surface area of 0.0119 km^2 (2.94 acres) and is about 154 m from the shoreline (Figure 6) (Google Earth Pro, 2021). Oleander Pond, located east of Alligator Lake (16R 395580.61 m E 3346681.81 m N), is about 135 m from the shoreline and has an estimated surface area of 0.0215 km^2 (5.31 acres). The depth of the lake and the pond is approximately one meter, and a 6 m dune system fronts the lake and west side of the pond while a 3 m dune system fronts the east side of the pond. The lake and pond are the study site and are of interest because they are potentially at risk of being contaminated by saltwater; this study specifically focuses on saltwater contamination through overtopping and overwashing.

Saltwater would not only contaminate the lake and pond but potentially contaminate the water-table aquifer since it is the shallowest aquifer at 13 m (O'Donnell, 2005) and may rely on recharge from the lake and pond (USGS, 2021). Eight wells providing freshwater on the east end of Dauphin Island exist approximately 11 m deep into the water-table aquifer with four wells (numbers 10, 20, 30, and 40) installed in 1990 and four additional (well numbers 50, 60, 70, and 80) installed in 1992 (Caldwell, 1996). Well #80 is approximately 334 m from Alligator Lake and may also be at risk of saltwater intrusion. The adaptation measure types, specifically the gulf beach measurement type from the Alabama Barrier Island Restoration Assessment Monitoring and Adaptive Management Plan, may benefit the study site since dune building will take place on the east end (Steyer et al., 2020). Increasing the elevation and width of the dunes could reduce the chances of dune overtopping and overwashing, and in turn reduce the likelihood of saltwater intrusion into the aquifer by those processes.

Figure 6. The high-resolution portion of the model domain (pink box) is shown including Alligator Lake and Oleander Pond (Google Earth Pro, 2021). The full model domain extends to the west, east, and offshore to a depth of 25.9 m to correspond to the depth at which waves were measured.

CHAPTER III

METHODOLOGY

3.1 XBeach

XBeach is a hydrodynamic and morphodynamic model that simulates changes to sand beaches by storms (Hoonhout, 2015). Hydrodynamic operations include short and long wave transformations, wave setup, unsteady currents, and inundation. Morphodynamic operations include sediment transport by suspended loads and bed loads, dune collapsing, overwash, and breaching. XBeach computes coupled 2D horizontal equations for wave propagation, flow, sediment transport and bottom changes, and spectral wave and flow boundary conditions. The model also applies shallow water equations such as the mass balance and momentum balance equations using a finite volume approach. XBeach uses a world coordinate system with the *x*-coordinate in cross-shore direction and the *y*-coordinate in the longshore direction. The model requires a curvilinear grid and can use local coordinates relative to world coordinates based on an origin and an orientation for a rectangular grid. The grid uses an offset/alternating approach with bed levels, water levels, water depths and concentrations designated at cell centers and velocities and sediment transport designated at cell nodes.

3.2 General grid and model setup

Merged digital elevation model (DEM) (OCM Partners, 2022a) and light detection and ranging (LiDAR) 2016 data (OCM Partners, 2022b) projected in UTM coordinates were obtained from Office for Coastal Management Partners and used to

create a model domain. The DEM and LiDAR data represent bathymetry and topography for the study site (Posey, 2021). The resolutions of the DEM and LiDAR data were one meter and ten meters. The horizontal and vertical accuracies of the bathymetric DEM data are a function of depth (d). The horizontal accuracy of the bathymetric DEM data was 3.5 + 0.05d m. The shallow and deep -water vertical accuracies for bathymetric DEM data were $\sqrt{0.20^2 + 0.0075d^2}$m and $\sqrt{0.30^2 + 0.013d^2}$ m. The horizontal and vertical accuracies of the topographic LiDAR data were one meter and 19.6 cm. A grid with 524 cells in the *x* direction and 766 cells in the *y* direction containing Alligator Lake and Oleander Pond was created using MATLAB code (MATLAB, 2019) (Figure 7). The grid was rotated by 90 degrees to accommodate a south-facing beach for Dauphin Island. To reduce computational time, the grid resolution, which refers to the grid cell spacing, was set to vary spatially, with high-resolution used at and in the nearshore region of Alligator Lake and Oleander Pond and low resolution used at the offshore region and at the lateral boundaries. High, middle, and low resolutions within the grid were spaced one meter, twenty meters, and fifty meters, respectively. The grid is spatially varying with higher resolution in front of Alligator Lake and Oleander Pond while lower resolution exists at the lateral boundaries and in the offshore direction. The offshore depth of the grid was set to 25.9 m, corresponding to the depth of National Oceanic and Atmospheric Administration (NOAA) data buoy station 42012 (NOAA-NDBC, 2017a) Specifically, the DEM and LiDAR data were used at an elevation of -4.5 m, corresponding to where the depth levels off (Figure 8). The elevation was artificially extended -25.9 m using a slope of 1/100 to reduce computational speed while still allowing XBeach to transform waves to the nearshore. Spectral wave data during Hurricane Nate from this buoy were

applied as the offshore boundary wave conditions in XBeach (Figure 3), and XBeach simulated onshore wave transformations. The waves recorded from data buoy station 42012 are likely not fully representative of waves that propagate from south of Dauphin Island because the waves from the data buoy are likely affected by the ebb tidal delta.

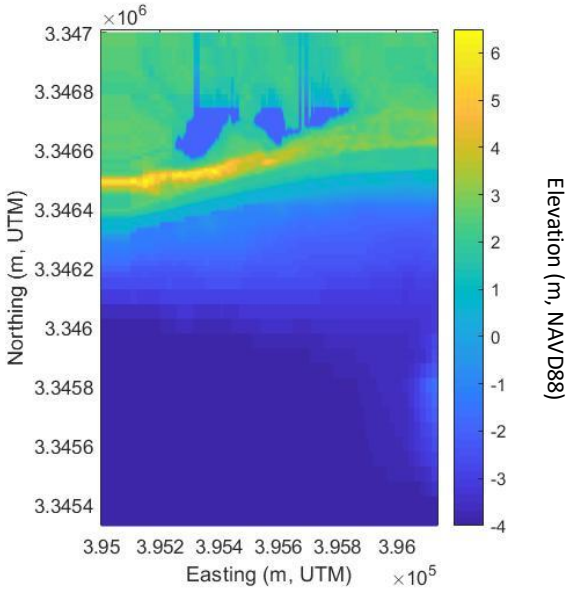

Figure 7. Bathymetry (color bar) is in meters with Alligator Lake to the west behind a dune system of approximately 6 m and Oleander Pond (U-shaped). Note that the offshore depth (25.9 m) is not shown in this grid although waves were simulated from this depth. Vertical streaks at the top of Alligator Lake and Oleander Pond are connecting tributaries displayed in the grid because they matched the minimum elevation used to identify the lake and pond within the topography dataset; the lake and pond were set to -2 m so that XBeach would recognize the lake and pond as water.

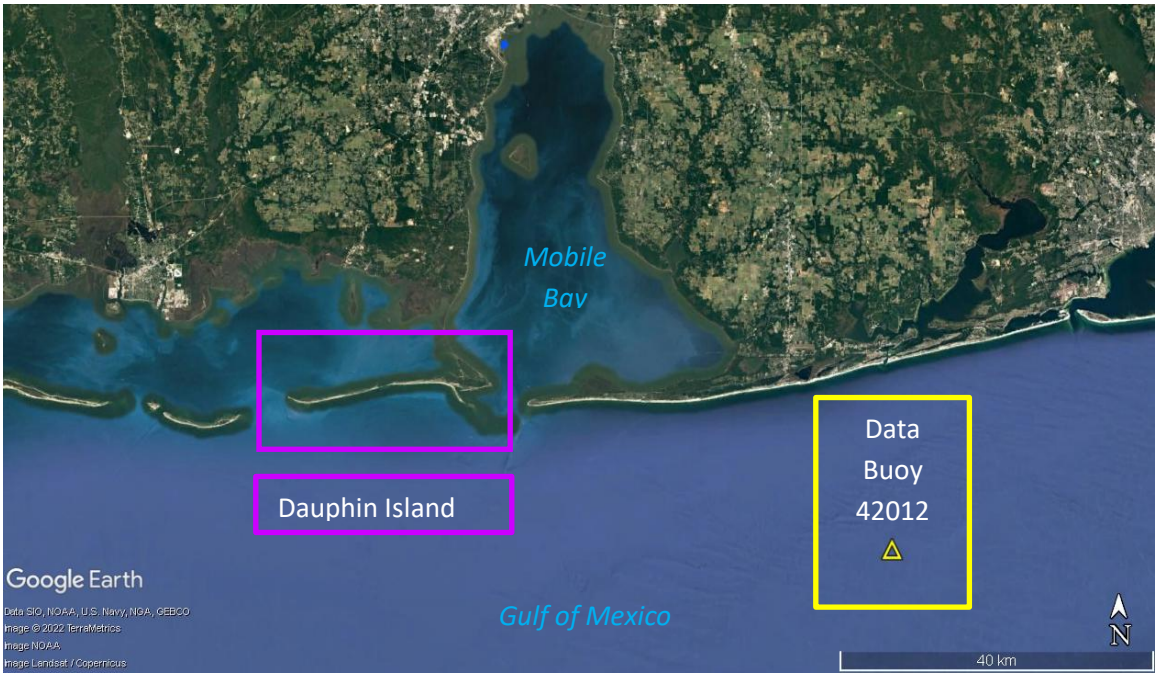

Figure 8. Dauphin Island is shown with respect to the location of NOAA data buoy station 42012. Note that this is the current location of the data buoy deployed at depth of 23.5 m; the depth of the data buoy during Hurricane Nate was 25.9 m.

The *facua* parameter affects sediment transport and allows wave skewness and asymmetry directed flows to be specified at once (Hoonhout, 2015) Although the default for the *facua* parameter is 0.1, this parameter was set to 0.01 because it was most representative of sediment transport at Dauphin Island (Posey, 2021). Land elevations and bathymetry were simulated with a bed file estimating Alligator Lake and Oleander Pond at elevation of -2 m using North American Vertical Datum of 1988 (NAVD88). This estimated elevation was used so that XBeach would recognize the lake and pond as water rather than land. Manning's roughness coefficient was used as a model input to represent friction losses due to land cover or water. Roughness coefficient values from Passeri et al. (2018) were used for open water (n = 0.022), bare land (n = 0.03), and

estuarine forested wetland (n = 0.15) to create a land cover/water text file for the grid. MATLAB code was used to create the text file to represent land cover and water for the grid (MATLAB, 2019).

3.3 Adaptation strategies

The existing condition adaptation strategy is routine beach nourishment to preserve beach profiles as they erode and evolve due to SLR (Figure 9). Cross-shore profiles were plotted through Alligator Lake (Transect A: 395325 m E) and the west (Transect B: 395600 m E) and east (Transect C: 395600 m E) side of Oleander Pond to represent elevations and compare bed level changes within the grid (Figure 10). Each cross-shore transect was drawn through the lake and the pond at locations with the narrowest beach width. It was assumed that profiles remained constant with SLR.

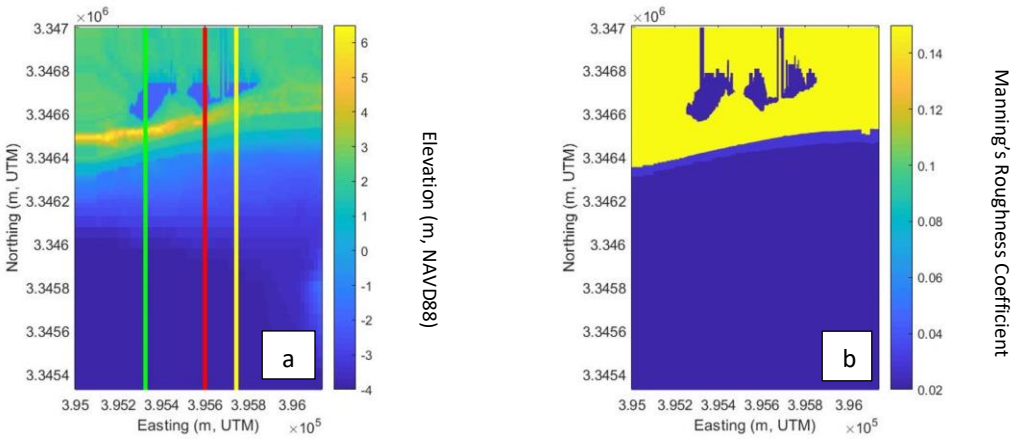

Figure 9. (a) Initial bathymetry (color bar) is in meters with Alligator Lake to the west behind a dune system of approximately 6 m and Oleander Pond (U-shaped) to the east for existing condition including Transects A, B, and C (green, red, and yellow lines). (b) Manning's roughness coefficients (color bar) were used to represent land cover (n = 0.03 and n = 0.15) and water (n = 0.022) for existing condition.

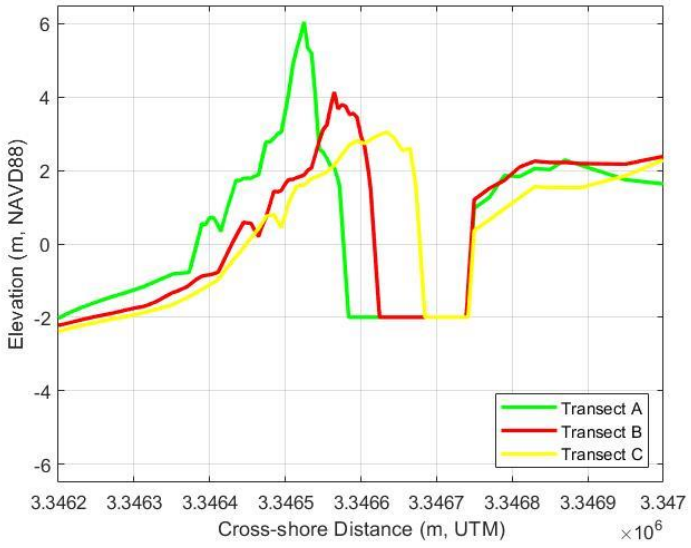

Figure 10. From Transects A, B, and C, the cross-shore profiles (green, red, and yellow lines) are plotted as elevation with respect to cross-shore distance for existing condition.

A second 524 x 766 grid was created to represent a beach nourishment with a larger sediment volume as an adaptation strategy to SLR instead of routine maintenance. The grid used the same domain and range as the existing condition adaptation strategy. Initial bathymetry for increased beach width (Strategy 1) revealed that the highest elevation exceeded six meters and existed in front of Alligator Lake to the west side of Oleander Pond (Figure 11). Lower elevations at approximately three meters were present in front of the right side of Oleander Pond. Strategy 1 simulated in this study was taken as an average value from a range of widths being considered by a coastal engineering firm to nourish the east end of Dauphin Island. The beach width was extended to 70 m (B. Webb, personal communication, November 11, 2021) while the beach elevation remained at 1 m. The beach was set to a slope of 0.06 (approximately 1:17) to avoid a vertical drop from the beach to the nearshore region. This slope was used instead of a steeper slope (approximately 1:10) because the grid resolution required a gentler slope to represent a realistic beach slope for Dauphin Island. The extended beach was accounted for by changing existing water (n = 0.022) to bare land (n = 0.03) (Figure 12). Cross-shore profiles were plotted through Transects A, B, and C to represent elevations and compare bed level changes within the grid (Figure 13).

A third 524 x 766 grid for increased beach elevation and increased width (Strategy 2) was created using the same domain and range for the grid with existing condition adaptation strategy. Initial bathymetry for Strategy 2 revealed that the highest elevation exceeded six meters and existed in front of Alligator Lake to the left side of Oleander Pond (Figure 11). Lower elevations at approximately three meters were present in front of the right side of Oleander Pond. The beach elevation used for this adaptation

strategy was adapted from an engineering firm that intends to implement this elevation for the berms on the east end of Dauphin Island. The beach width was extended to 70 m while the beach elevation was raised to 1.83 m (B. Webb, personal communication November 11, 2021). Manning's roughness coefficient for the raised and widened beach was changed from n = 0.022 (open water) to n = 0.03 (bare land) to account for additional sand where water previously existed (Figure 12). Cross-shore profiles were plotted through Transects A, B, and C to represent elevations and compare bed level changes within the grid (Figure 13). Strategy 3 intends to increase the elevation of the beach and dunes and increase the beach width but was not simulated in this study. However, it was included in the AP for the study site.

Figure 11. Initial bathymetry (color bar) is in meters with Alligator Lake to the west behind a dune system of approximately 6 m and Oleander Pond (U-shaped) to the east including Transects A, B, and C (green, red, and yellow lines) for (a) existing condition, (b) Strategy 1, and (c) Strategy 2. Positive values represent land while negative values represent water.

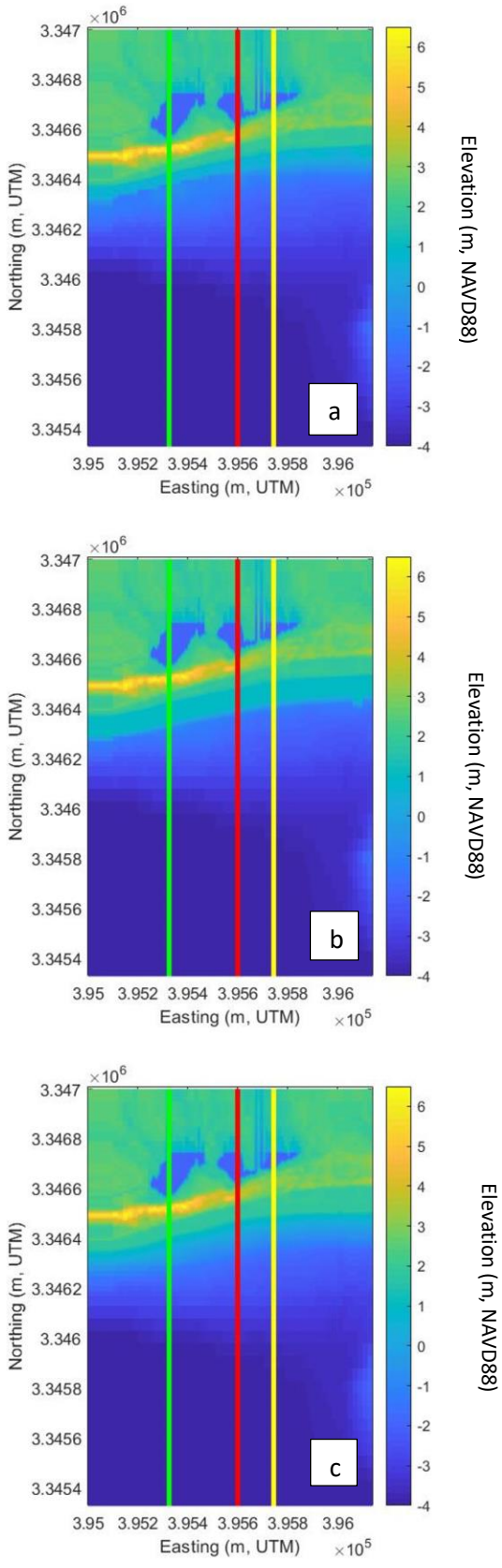
×10^6
3.347
3.3468
3.3466
3.3464
3.3462
3.346
3.3458
3.3456
3.3454
Northing (m, UTM)
3.95 3.952 3.954 3.956 3.958 3.96
Easting (m, UTM)
×10^5
6 5 4 3 2 1 0 -1 -2 -3 -4
Elevation (m, NAVD88)
a
b
c

Figure 12. Manning's roughness coefficients (color bar) were used to represent land cover (n = 0.03 and n = 0.15) and water (n = 0.022) for (a) existing condition, (b) Strategy 1, and (c) Strategy 2.

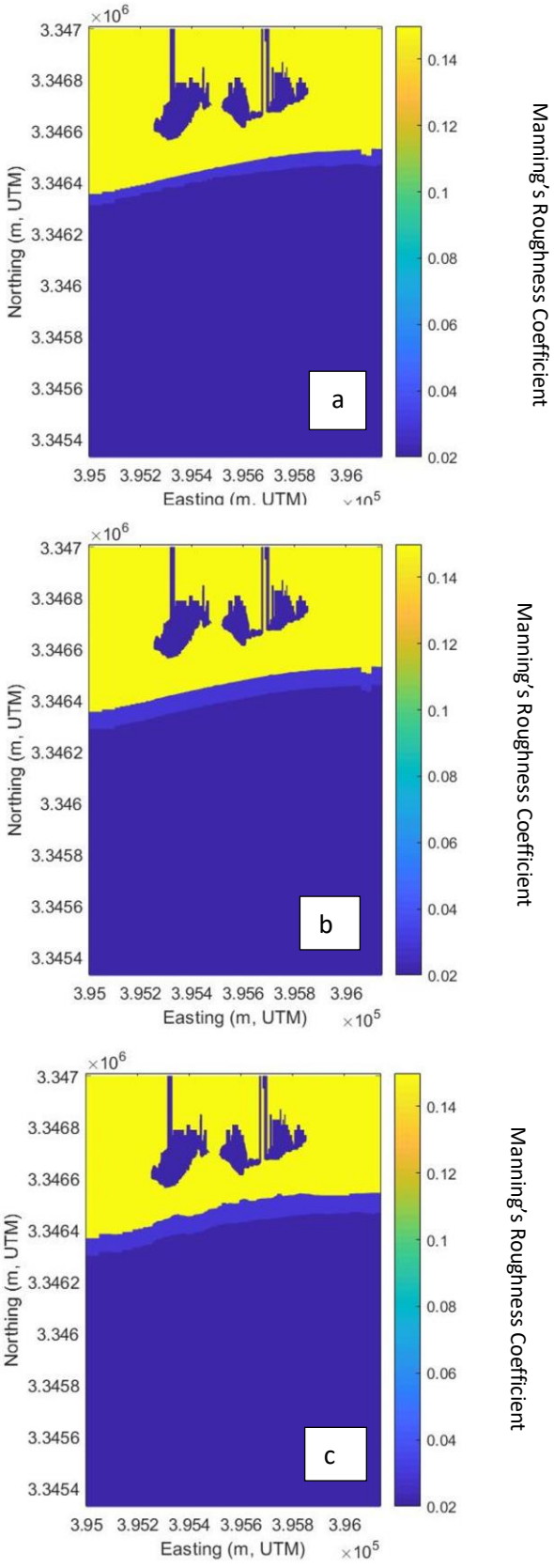
×10^6
3.347
3.3468
3.3466
3.3464
3.3462
3.346
3.3458
3.3456
3.3454
Northing (m, UTM)
3.95 3.952 3.954 3.956 3.958 3.96
Easting (m, UTM)
×10^5
0.14
0.12
0.1
0.08
0.06
0.04
0.02
Manning's Roughness Coefficient
a
b
c

Figure 13. Cross-shore profiles were plotted as elevation with respect to cross-shore distance for (a) Transect A, (b) Transect B, and (c) Transect C for existing condition (black line), Strategy 1 (pink line), and Strategy 2 (blue line).

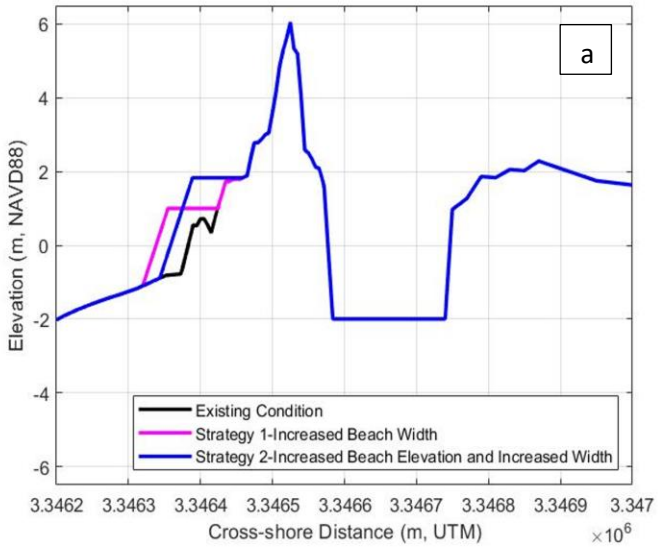
a
Elevation (m, NAVD88)
Cross-shore Distance (m, UTM)
×10^6
Existing Condition
Strategy 1-Increased Beach Width
Strategy 2-Increased Beach Elevation and Increased Width

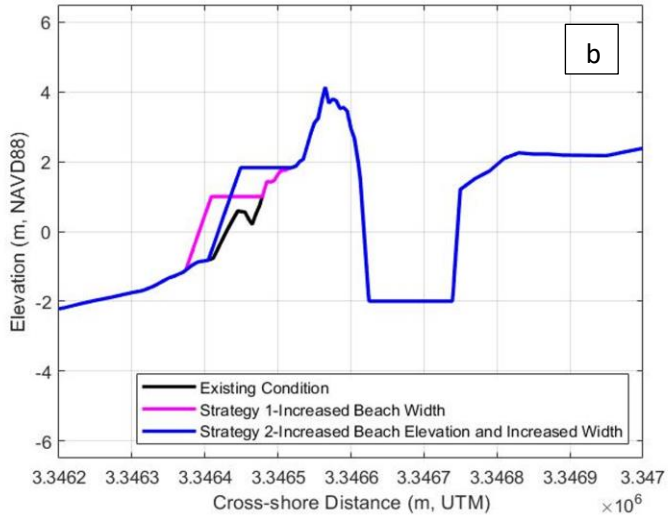
b
Elevation (m, NAVD88)
Cross-shore Distance (m, UTM)
×10^6
Existing Condition
Strategy 1-Increased Beach Width
Strategy 2-Increased Beach Elevation and Increased Width

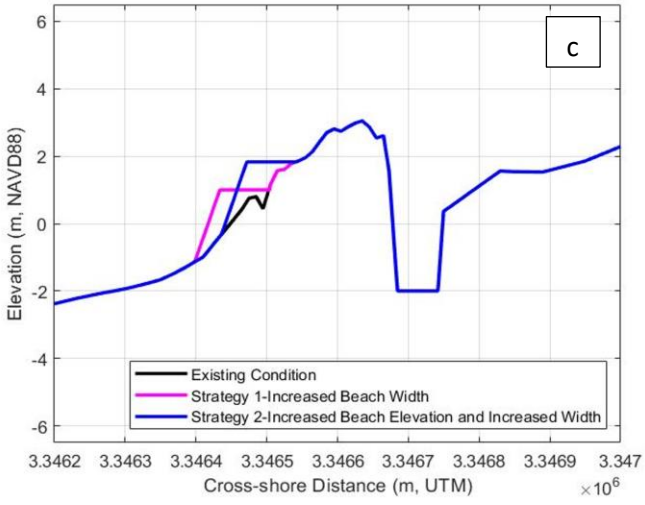
c
Elevation (m, NAVD88)
Cross-shore Distance (m, UTM)
×10^6
Existing Condition
Strategy 1-Increased Beach Width
Strategy 2-Increased Beach Elevation and Increased Width

3.4 Grid for land cover change around Alligator Lake and Oleander Pond

A fourth model setup was created to represent changing land cover around Alligator Lake and Oleander Pond. Land cover change around the lake and pond was not an adaptation strategy but was simulated to determine the impact vegetation around the lake and pond has on inundation extent. The land cover change around Alligator Lake and Oleander Pond was accounted for by changing the roughness coefficient of 0.15 (estuarine forested wetland) to 0.03 (bare land) for the Manning's grid (Figure 14). The elevation grid used for the existing condition adaptation strategy was used for land cover change around the lake and pond. Initial bathymetry for land cover change around Alligator Lake and Oleander Pond revealed that the highest elevation exceeded six meters and existed in front of Alligator Lake to the west side of Oleander Pond. Lower elevations at approximately three meters were present in front of the east side of Oleander Pond. The beach elevation was one meter.

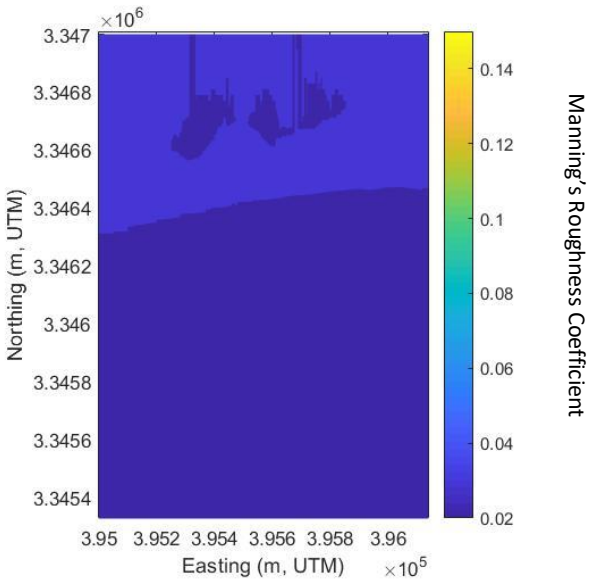

Figure 14. Manning's roughness coefficients (color bar) were used to represent land cover (n = 0.03) and water (n = 0.022) for land cover change.

3.5 SLR scenarios

Hurricane Nate water levels were obtained from Dauphin Island tide gauge 8735180 (NOAA-TC, 2017), and wave conditions were obtained from NOAA data buoy station 42012 (NOAA-NDBC, 2017). Sweet et al. (2017) projected global mean sea level (GMSL) rise scenarios for 2100 (low, intermediate-low, intermediate, intermediate-high, high, and extreme) which include 0.30 m, 0.50 m, 1.0 m, 1.5 m, 2.0 m, and 2.5 m. The SLR scenarios used in this study were adapted from Sweet et al. (2017) to represent relative SLR at Dauphin in Island in year 2100 which include 0.40 m, 0.53 m, 0.66 m, 0.75 m, 1.00 m, 1.26 m, and 1.93 m. The current mean sea level (MSL) at Dauphin Island is 0.016 m relative to NAVD88 (NOAA-TC, 2022b). The SLR scenarios were superimposed on Hurricane Nate water levels (Figure 15). Water levels from Hurricane

Nate without SLR were simulated to compare with simulations using Hurricane Nate water levels and superimposed SLR scenarios.

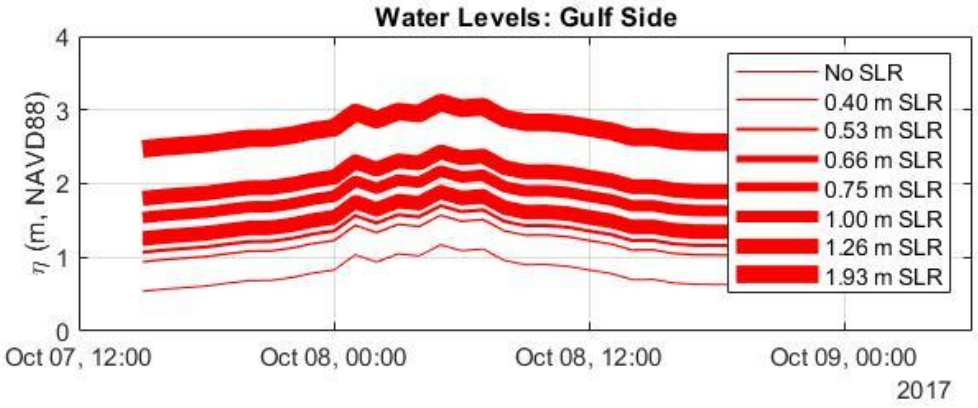

Figure 15. SLR scenarios were superimposed onto Hurricane Nate water levels from the Gulf of Mexico. No SLR (bottom red line) were actual water levels from Hurricane Nate while 1.93 m of SLR (top red line) was the maximum amount of SLR simulated in this study.

3.6 Inundation, total water levels, and cross-shore bathymetry

The total water levels simulated with XBeach were configured into an animation with bed elevations to determine areas within the model domain that submerged and areas that remained emergent (Figure 16a). A hydrograph animation with time (hr) as the *x*-axis and total water levels (m, NAVD88) as the *y*-axis was used to determine the timestep that peak water levels occurred (Figure 16b). An animation of cross-shore bathymetry and total water levels was used to determine if dune overtopping and erosion of the dune crest occurred (Figure 16c). In this study, it was inferred that saltwater

contaminated the lake and pond if dune overtopping occurred. Each animation was observed for no SLR and SLR scenarios at Transects A, B, and C.

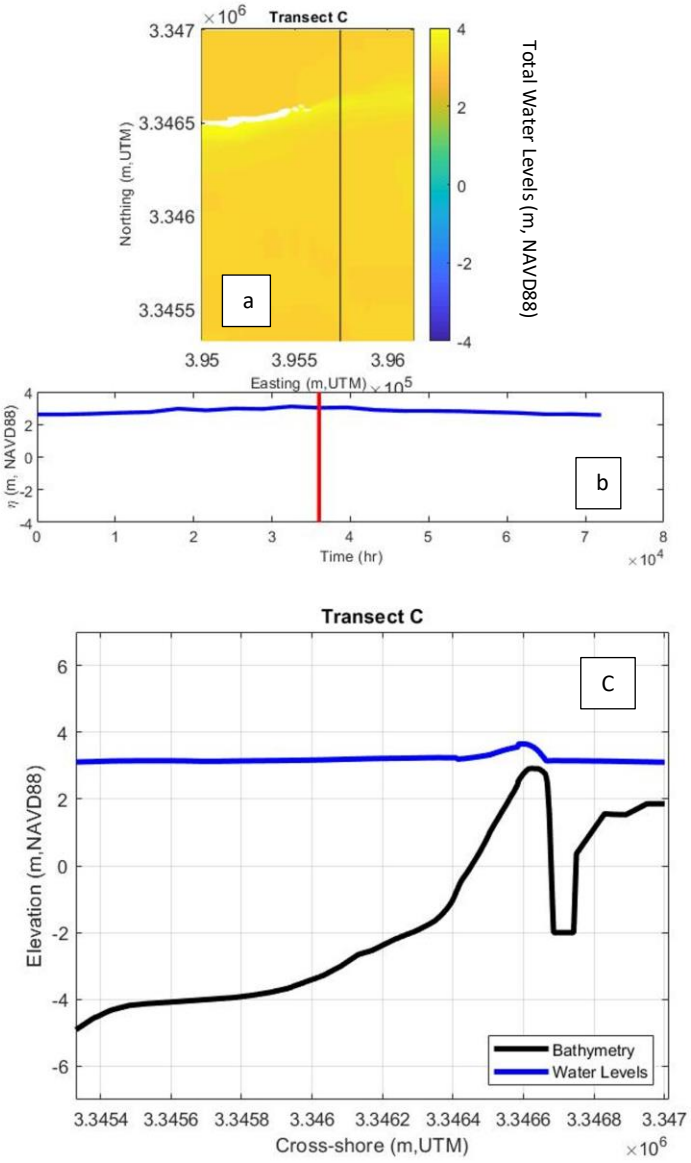

Figure 16. (a) The timestamp of total peak water levels (color bar) and bathymetry at Transect C shows areas that became inundated. Areas in white are emergent. (b) The timestamp of the hydrograph shows the timestep (red line) that peak water levels (blue line) occurred for Transect C. (c) The timestamp of cross-shore bathymetry (black line) and total water levels (blue line) is shown during peak water levels for Transect C. Note that these animations are shown for the existing condition adaptation strategy at 1.93 m of SLR.

CHAPTER IV

RESULTS

Model outputs for Hurricane Nate conditions and the sea level rise (SLR) scenarios were compared to determine if overtopping and topographic changes occurred near Alligator Lake and Oleander Pond. Saltwater intrusion in Alligator Lake may be estimated depending on the length and width of a breach and runup elevation. While breaching can occur due to overtopping (Kanning et al., 2007; Vorogushyn et al., 2009), breaching was not a concern in this study because of the beach width at the study site. Dune overtopping is a concern since total water levels could exceed the dune crest elevations armoring Alligator Lake and Oleander Pond. Erosion and deposition were quantified by taking the difference between pre-storm and post-storm bed elevations.

Elevation and water level data along three transects (A, B, and C) were extracted from the grids to compare difference in water levels with respect to dune elevations. Initial, peak, and final water levels were recorded by visual inspection as the maximum point at or near the dune from combined cross-shore bathymetry (initial and final) and total water level animations in MATLAB. The hydrographs were used to verify when the peak water levels occurred. Initial and final dune crest elevations were recorded by visual inspection as the maximum elevation of the dune. Water levels and dune crest elevations were obtained for each grid (existing condition, Strategy 1, Strategy 2, and land cover change around Alligator Lake and Oleander Pond) at no SLR and SLR scenarios (0.40, 0.53, 0.66, 0.75, 1.00, 1.26, and 1.93 m).

4.1 Adaptation strategies

For the existing condition adaptation strategy, no overtopping occurred at Alligator Lake (Transect A), and the final dune crest elevation was 6.05 m for all SLR scenarios. SLR of 0.00 m yielded the lowest peak water levels at 2.21 m while 1.93 m of SLR yielded the highest peak water levels at 4.26 m for Transect A (Table 1). At Transect B (west side of Oleander Pond), 0.00 m of SLR yielded lowest peak water levels at 2.08 m while 1.93 m of SLR yielded the highest peak water levels at 3.79 m (Table 2). Overtopping occurred at (Transect B) 1.93 m of SLR at the 3.75 hr timestep, indicating saltwater intrusion of Oleander Pond. The final dune crest elevation at 1.93 m of SLR was 3.65 m. At Transect C (east side of Oleander Pond), 0.00 m of SLR yielded the lowest peak water levels at 2.07 m while 1.93 m of SLR yielded the highest peak water levels at 3.65 m (Table 3). Overtopping occurred at 1.26 and 1.93 m of SLR at the 3.75 hr timestep, indicating saltwater intrusion of Oleander Pond at a lower SLR scenario for this transect. The final dune crest elevations at 1.26 and 1.93 m of SLR were 3.04 m and 2.97 m.

Table 1. Peak water levels and dune crest elevations were obtained from bathymetry/water level animations from Transect A for each SLR scenario (existing condition adaptation strategy).

SLR Scenario (m)	Initial Dune Crest Elevation (m)	Time Step of Overtopping (hr)	Peak Water Levels (m)	Final Dune Crest Elevation (m)
0.00	6.05	--	2.21	6.05
0.40	--	--	2.55	--
0.53	--	--	2.85	--
0.66	--	--	2.98	--
0.75		--	3.05	
1.00	--	--	3.28	--
1.26			3.47	
1.93	--	--	4.26	--

Table 2. Peak water levels and dune crest elevations were obtained from bathymetry/water level animations from Transect B for each SLR scenario (existing condition adaptation strategy).

SLR Scenario (m)	Initial Dune Crest Elevation (m)	Time Step of Overtopping (hr)	Peak Water Levels (m)	Final Dune Crest Elevation (m)
0.00	4.14	--	2.08	4.14
0.40	--	--	2.52	--
0.53	--	--	2.64	--
0.66	--	--	2.87	--
0.75	--	--	2.93	--
1.00	--	--	3.22	--
1.26	--	--	3.28	--
1.93	4.14	3.75	3.79	3.65

Table 3. Peak water levels and dune crest elevations were obtained from bathymetry/water level animations from Transect C for each SLR scenario (existing condition adaptation strategy).

SLR Scenario (m)	Initial Dune Crest Elevation (m)	Time Step of Overtopping (hr)	Peak Water Levels (m)	Final Dune Crest Elevation (m)
0.00	3.05	--	2.07	3.05
0.40	--	--	2.46	--
0.53	--	--	2.63	--
0.66	--	--	2.75	--
0.75	--	--	2.80	--
1.00	--	--	2.97	--
1.26	--	3.75	3.17	3.04
1.93	--	3.75	3.65	2.97

For Strategy 1, no overtopping occurred at Alligator Lake (Transect A), and the final dune crest elevation was 6.05 m for all SLR scenarios. SLR of 0.00 m yielded the lowest peak water levels at 2.08 m while 1.93 m of SLR yielded the highest peak water levels at 4.09 m for Transect A (Table 4). At Transect B (west side of Oleander Pond), 0.00 m of SLR yielded the lowest peak water levels at 2.01 m while 1.93 m of SLR yielded the highest peak water levels at 3.79 m (Table 5). Overtopping occurred at (Transect B) 1.93 m of SLR at the 3.75 hr timestep, indicating saltwater intrusion of Oleander Pond. The final dune crest elevation at 1.93 m of SLR was 3.76 m. At Transect C (east side of Oleander Pond), 0.00 m of SLR yielded the lowest peak water levels at 2.02 m while 1.93 m of SLR yielded the highest peak water levels at 3.61 m (Table 6). Overtopping occurred at the 3.75 hr timestep, indicating saltwater intrusion of Oleander Pond at a lower SLR scenario for this transect. The final dune crest elevations at 1.26 and 1.93 m of SLR were 3.05 and 2.96 m.

Table 4. Peak water levels and dune crest elevations were obtained from bathymetry/water level animations from Transect A for each SLR scenario (Strategy 1).

SLR Scenario (m)	Initial Dune Crest Elevation (m)	Time Step of Overtopping (hr)	Peak Water Levels (m)	Final Dune Crest Elevation (m)
0.00	6.05	--	2.08	6.05
0.40	--	--	2.51	--
0.53	--	--	2.63	--
0.66	--	--	2.85	--
0.75			2.96	
1.00	--	--	3.26	--
1.26	--	--	3.43	--
1.93			4.09	

Table 5. Peak water levels and dune crest elevations were obtained from bathymetry/water level animations from Transect B for each SLR scenario (Strategy 1).

SLR Scenario (m)	Initial Dune Crest Elevation (m)	Time Step of Overtopping (hr)	Peak Water Levels (m)	Final Dune Crest Elevation (m)
0.00	4.14	--	2.01	4.14
0.40	--	--	2.49	--
0.53	--	--	2.61	--
0.66	--	--	2.70	--
0.75	--		2.82	--
1.00	--	--	3.22	--
1.26	--	--	3.23	--
1.93	--	--	3.79	

Table 6. Peak water levels and dune crest elevations were obtained from bathymetry/water level animations from Transect C for each SLR scenario (Strategy 1).

SLR Scenario (m)	Initial Dune Crest Elevation (m)	Time Step of Overtopping (hr)	Peak Water Levels (m)	Final Dune Crest Elevation (m)
0.00	3.05	--	2.02	3.05
0.40	--	--	2.41	--
0.53	--	--	2.55	--
0.66	--	--	2.71	--
0.75	--	--	2.77	--
1.00	--	--	2.94	--
1.26	--	3.75	3.14	3.05
1.93	--	3.75	3.61	2.96

For Strategy 2, no overtopping occurred at Alligator Lake (Transect A), and the final dune crest elevation was 6.05 m for all SLR scenarios. SLR at 0.00 m yielded the lowest peak water levels at 1.91 m while 1.93 m of SLR yielded the highest peak water levels at 4.03 m for Transect A (Table 7). At Transect B (west side of Oleander Pond), 0.00 m of SLR yielded the lowest peak water levels at 2.01 m while 1.93 m of SLR yielded the highest peak water levels at 3.80 m (Table 8). Overtopping occurred at (Transect B) 1.93 m of SLR at the 3.75 hr timestep, indicating saltwater intrusion of Oleander Pond. The final dune crest elevation was 3.79 m. At Transect C (east side of Oleander Pond), 0.00 m of SLR yielded the lowest peak water levels at 2.04 m while 1.93 m of SLR yielded the highest peak water levels at 3.61 m (Table 9). Overtopping occurred at 1.26 and 1.93 m of SLR at the 3.75 hr timestep, indicating saltwater intrusion of Oleander Pond at a lower SLR scenario for this transect. The final dune crest elevations at 1.26 and 1.93 m of SLR were 3.04 and 2.93 m.

Table 7. Peak water levels and dune crest elevations were obtained from bathymetry/water level animations from Transect A for each SLR scenario (Strategy 2).

SLR Scenario (m)	Initial Dune Crest Elevation (m)	Time Step of Overtopping (hr)	Peak Water Levels (m)	Final Dune Crest Elevation (m)
0.00	6.05	--	1.91	6.05
0.40	--	--	2.52	--
0.53	--	--	2.60	--
0.66	--	--	2.83	--
0.75	--	--	2.95	--
1.00	--	--	3.23	--
1.26	--	--	3.38	--
1.93	--	--	4.03	--

Table 8. Peak water levels and dune crest elevations were obtained from bathymetry/water level animations from Transect B for each SLR scenario (Strategy 2).

SLR Scenario (m)	Initial Dune Crest Elevation (m)	Time Step of Overtopping (hr)	Peak Water Levels (m)	Final Dune Crest Elevation (m)
0.00	4.14	--	2.01	4.14
0.40	--	--	2.50	--
0.53	--	--	2.63	--
0.66	--	--	2.80	--
0.75	--	--	2.93	--
1.00	--	--	3.25	--
1.26	--	--	3.19	--
1.93	--	--	3.80	--

Table 9. Peak water levels and dune crest elevations were obtained from bathymetry/water level animations from Transect C for each SLR scenario (Strategy 2).

SLR Scenario (m)	Initial Dune Crest Elevation (m)	Time Step of Overtopping (hr)	Peak Water Levels (m)	Final Dune Crest Elevation (m)
0.00	3.05	--	2.04	3.05
0.40	--	--	2.38	--
0.53	--	--	2.57	--
0.66	--	--	2.77	--
0.75	--	--	2.79	--
1.00	--	--	2.95	--
1.26	--	3.75	3.13	3.04
1.93	--	3.75	3.61	2.93

For the existing condition adaptation strategy, final bathymetry for no SLR yielded the same elevations as initial bathymetry except at the beach where elevations and width decreased (Figure 17). Change in bathymetry revealed 0.5 m of deposition in the nearshore zone (395412 m E 3346388 m N), and -0.5 m of erosion at the beach (395396 m E 3346451 m N) (Figure 18). A larger magnitude of deposition occurred in front of Alligator Lake and the west side of Oleander Pond (0.5 m) than the east side of Oleander Pond (0.4 m). Deposition extent was 23 m, and erosion extent was 68 m in front of the east side of Oleander Pond. Deposition was present around the perimeters of the lake and pond, especially at the north end of Oleander Pond.

For Strategy 1, final bathymetry for no SLR yielded the same elevations as initial bathymetry except at the beach where elevations and width decreased (Figure 17). Change in bathymetry revealed 0.5 m of deposition in the nearshore zone (395412 m E 3346388 m N), and -0.5 m of erosion at the beach (395396 m E 3346451 m N) (Figure 18). Strategy 1 yielded a greater magnitude of deposition (0.5 m) and greater extent and

continuation of deposition (51 m) in front of the east side of Oleander Pond. Less extent of erosion (44 m) occurred in front of the east side of Oleander Pond compared to existing condition adaptation strategy. Deposition was present around the perimeters of the lake and pond, especially at the north end of Oleander Pond.

For Strategy 2, final bathymetry for no SLR yielded the same elevations as initial bathymetry except at the beach where elevations and width decreased (Figure 17). Change in bathymetry revealed 0.5 m of deposition in the nearshore zone (395412 m E 3346388 m N), and -0.5 m of erosion at the beach (395396 m E 3346451 m N) (Figure 18). Strategy 2 yielded a greater extent of deposition (74 m) in front of the east side of Oleander Pond compared to existing condition and Strategy 1. Erosion extent was slightly greater (50 m) than Strategy 1 but still less than existing condition. Deposition was present around the perimeters of the lake and pond, especially at the north end of Oleander Pond. More investigation is needed to determine the cause of this sediment transport in the lake and pond.

Figure 17. Final bathymetry for no SLR was plotted for (a) existing condition, (b) Strategy 1, and (c) Strategy 2 including Transects A, B, and C (green, red, and yellow lines). Positive values represent land while negative values represent water.

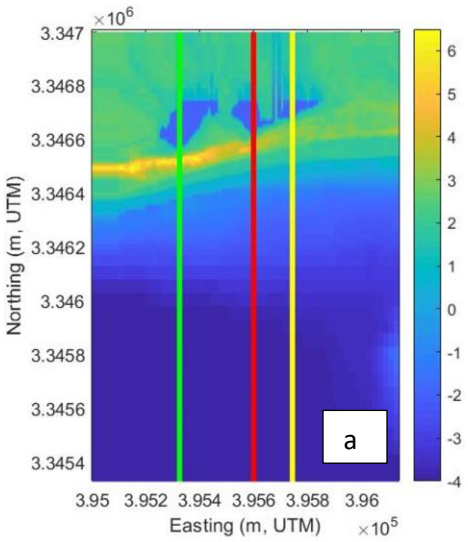
×10^6
3.347
3.3468
3.3466
3.3464
3.3462
3.346
3.3458
3.3456
3.3454
Northing (m, UTM)
6
5
4
3
2
1
0
-1
-2
-3
-4
a
3.95 3.952 3.954 3.956 3.958 3.96
Easting (m, UTM)
×10^5

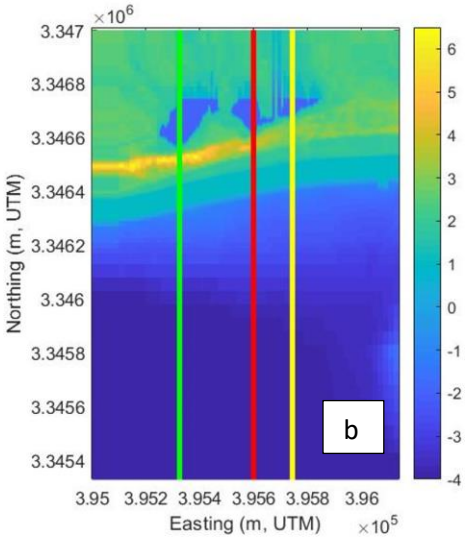
×10^6
3.347
3.3468
3.3466
3.3464
3.3462
3.346
3.3458
3.3456
3.3454
Northing (m, UTM)
6
5
4
3
2
1
0
-1
-2
-3
-4
b
3.95 3.952 3.954 3.956 3.958 3.96
Easting (m, UTM)
×10^5

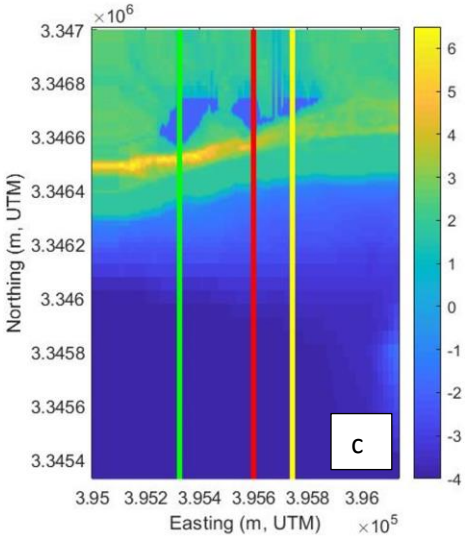
×10^6
3.347
3.3468
3.3466
3.3464
3.3462
3.346
3.3458
3.3456
3.3454
Northing (m, UTM)
6
5
4
3
2
1
0
-1
-2
-3
-4
c
3.95 3.952 3.954 3.956 3.958 3.96
Easting (m, UTM)
×10^5

Figure 18. Change in bathymetry for no SLR was plotted for (a) existing condition, (b) Strategy 1, and (c) Strategy 2 including Transects A, B, and C (green, red, and yellow lines). Positive values represent deposition while negative values represent erosion.

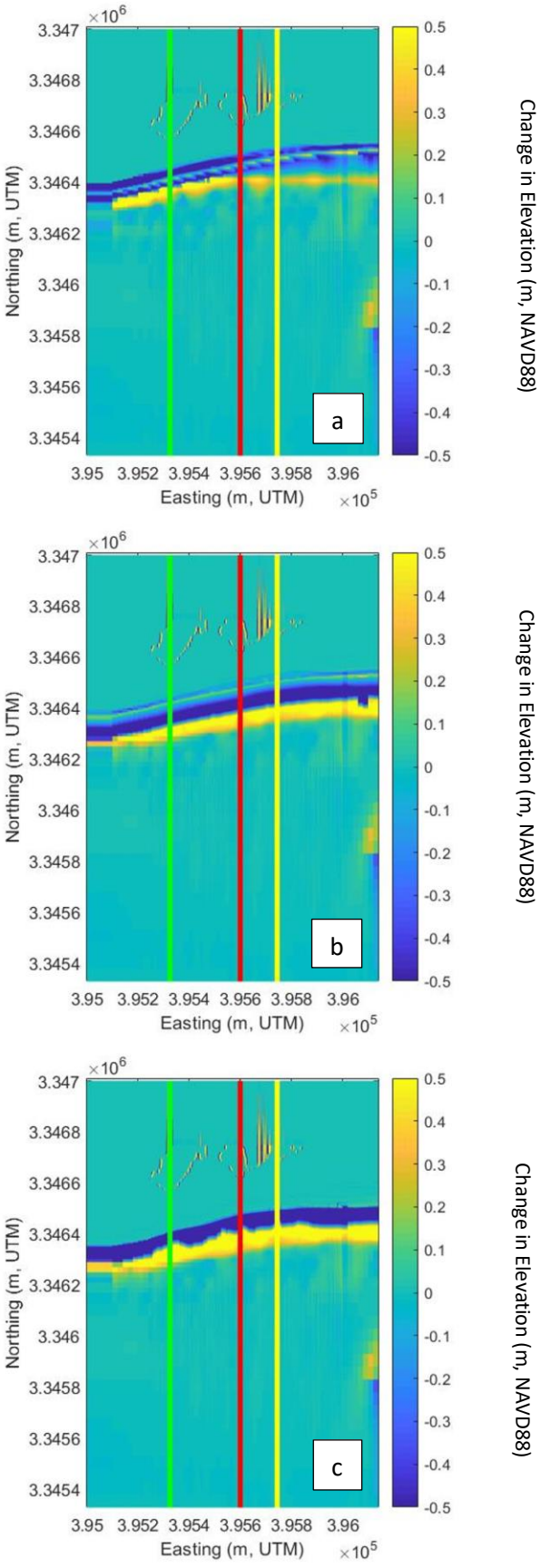
×10^6
3.347
3.3468
3.3466
3.3464
3.3462
3.346
3.3458
3.3456
3.3454
Northing (m, UTM)
3.95 3.952 3.954 3.956 3.958 3.96
Easting (m, UTM)
×10^5
0.5
0.4
0.3
0.2
0.1
0
-0.1
-0.2
-0.3
-0.4
-0.5
Change in Elevation (m, NAVD88)
a
b
c

4.2 Land cover change around Alligator Lake and Oleander Pond

For changing land cover around Alligator Lake and Oleander Pond, no overtopping occurred at Alligator Lake (Transect A), and the final dune crest elevation was 6.05 m for all SLR scenarios. SLR of 0.00 m yielded the lowest peak water levels at 2.16 m while 1.93 m of SLR yielded the highest peak water levels at 3.81 m for Transect A (Table 10). At Transect B (west side of Oleander Pond), 0.00 m of SLR yielded the lowest peak water levels at 2.17 m while 1.93 m of SLR yielded the highest peak water levels at 3.81 m (Table 11). Overtopping occurred at (Transect B) 1.93 m of SLR at the 3.75 hr timestep, indicating saltwater intrusion of Oleander Pond. The final dune crest elevation at 1.93 m of SLR was 3.76 m. At Transect C (east side of Oleander Pond), 0.00 m of SLR yielded the lowest peak water levels at 2.17 m while 1.93 m of SLR yielded the highest peak water levels at 3.42 m (Table 12). Overtopping occurred at 1.00, 1.26, and 1.93 m of SLR at the 3.75 hr timestep, indicating saltwater intrusion of Oleander Pond at a lower SLR scenario for this transect. The final dune crest elevations at 1.00, 1.26, and 1.93 m of SLR were 3.05, 2.99, and 2.34 m.

Table 10. Peak water levels and dune crest elevations were obtained from bathymetry/water level animations from Transect A for each SLR scenario (land cover change).

SLR Scenario (m)	Initial Dune Crest Elevation (m)	Time Step of Overtopping (hr)	Peak Water Levels (m)	Final Dune Crest Elevation (m)
0.00	6.05	--	2.16	6.05
0.40	--	--	2.37	--
0.53	--	--	2.51	--
0.66	--	--	2.70	--
0.75	--	--	2.93	--
1.00	--	--	3.14	--
1.26	--	--	3.25	--
1.93	--	--	3.81	--

Table 11. Peak water levels and dune crest elevations were obtained from bathymetry/water level animations from Transect B for each SLR scenario (land cover change).

SLR Scenario (m)	Initial Dune Crest Elevation (m)	Time Step of Overtopping (hr)	Peak Water Levels (m)	Final Dune Crest Elevation (m)
0.00	--	2.17	4.14	--
0.40	--	2.46	--	--
0.53	--	2.60	--	--
0.66	--	2.73	--	--
0.75	--	2.63	--	--
1.00	--	2.81	--	--
1.26	--	3.12	--	--
1.93	--	3.77	--	--

Table 12. Peak water levels and dune crest elevations were obtained from bathymetry/water level animations from Transect C for each SLR scenario (land cover change).

SLR Scenario (m)	Initial Dune Crest Elevation (m)	Time Step of Overtopping (hr)	Peak Water Levels (m)	Final Dune Crest Elevation (m)
0.00	3.05	--	2.17	3.05
0.40	--	--	2.66	--
0.53	--	--	2.76	--
0.66	--	--	2.78	--
0.75	--	--	2.88	--
1.00	--	3.75	3.05	3.05
1.26	--	3.75	3.12	2.99
1.93	--	3.75	3.42	2.34

For changing land cover around Alligator Lake and Oleander Pond, final bathymetry for no SLR yielded the same elevations as initial bathymetry except at the beach where elevations and width decreased (Figure 19). Change in bathymetry yielded the same deposition and erosion patterns as existing condition. A larger magnitude of deposition occurred in front of Alligator Lake and the west side of Oleander Pond (0.5 m) than the right side of Oleander Pond (0.4 m). Deposition extent was 23 m, and erosion extent was 68 m in front of the east side of Oleander Pond. Deposition was present around the perimeters of the lake and pond, especially at the north end of Oleander Pond.

Figure 19. (a) Initial, (b) final, and (c) change in bathymetry were plotted for land cover change around Alligator Lake and Oleander Pond including Transects A, B, and C (green, red, and yellow lines). Positive values for initial and final bathymetry represent land while negative values represent water. Positive values for change in bathymetry represent deposition while negative values represent erosion.

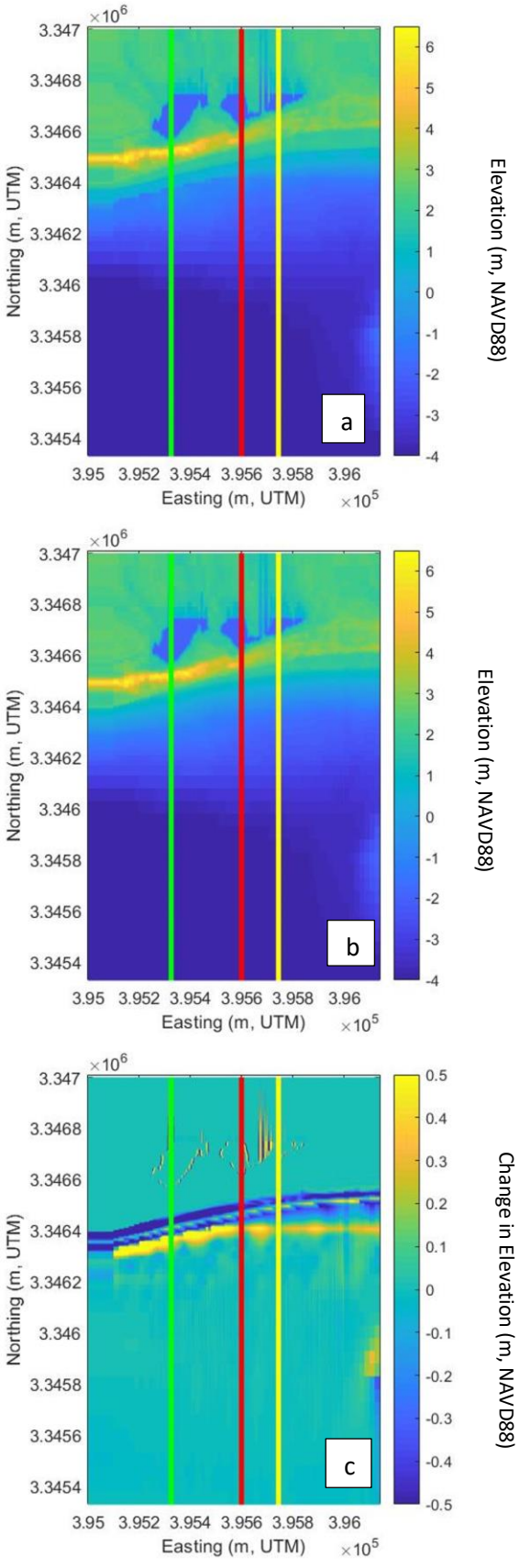
×10^6
3.347
3.3468
3.3466
3.3464
3.3462
3.346
3.3458
3.3456
3.3454
Northing (m, UTM)
3.95 3.952 3.954 3.956 3.958 3.96
Easting (m, UTM)
×10^5
6
5
4
3
2
1
0
-1
-2
-3
-4
Elevation (m, NAVD88)
a
b
c
0.5
0.4
0.3
0.2
0.1
0
-0.1
-0.2
-0.3
-0.4
-0.5
Change in Elevation (m, NAVD88)

4.3 Water level and dune crest elevation comparisons

Peak water levels from XBeach outputs were plotted with SLR scenarios for existing condition, Strategy 1, Strategy 2, and land cover change around Alligator Lake and Oleander Pond (Figure 20). The plots were used to determine adaptation strategy effectiveness in reducing inundation by overtopping. From Transect A, Strategy 2 yielded the lowest peak water levels (1.91 m) at no SLR while land cover change around Alligator Lake and Oleander Pond yielded lowest water peak levels for all other SLR scenarios. From Transect B, Strategies 1 and 2 yielded the lowest peak water levels (2.01 m) at no SLR. Land cover change around Alligator Lake and Oleander Pond yielded the lowest peak water levels at all other SLR scenarios except at 0.66 m of SLR with Strategy 1 yielding the lowest peak water levels. From Transect C, Strategy 1 yielded the lowest peak water levels (2.02 m) at no SLR. All other SLR scenarios yielded the lowest peak water levels from Strategies 1 or 2 except at 1.93 m of SLR with land cover change around Alligator Lake and Oleander Pond yielding the lowest peak water levels (3.42 m).

Figure 20. Peak water levels were plotted with SLR for existing condition (purple bar), Strategy1 (gold bar), Strategy 2 (pink bar), and land cover change around Alligator Lake and Oleander Pond (blue bar) for Transects A, B, and C. Note that land cover change around Alligator Lake and Oleander Pond is not an adaptation strategy.

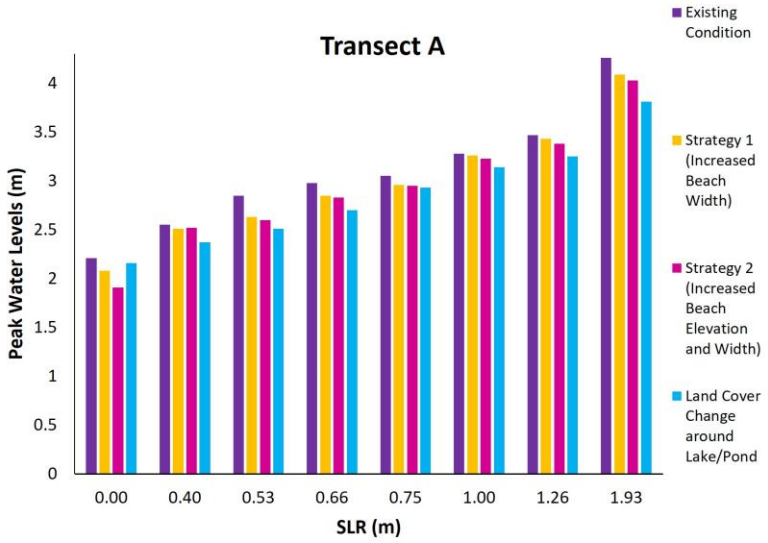
Transect A
Peak Water Levels (m)
0
0.5
1
1.5
2
2.5
3
3.5
4
0.00
0.40
0.53
0.66
0.75
1.00
1.26
1.93
SLR (m)
Existing Condition
Strategy 1 (Increased Beach Width)
Strategy 2 (Increased Beach Elevation and Width)
Land Cover Change around Lake/Pond

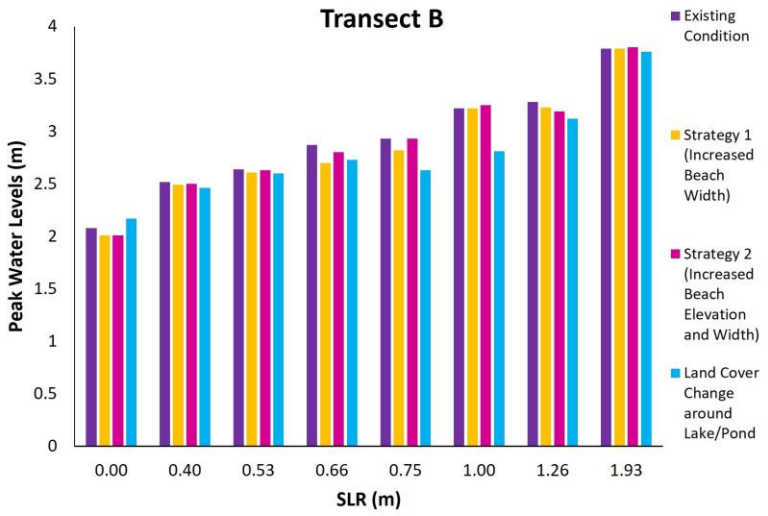
Transect B
Peak Water Levels (m)
0
0.5
1
1.5
2
2.5
3
3.5
4
0.00
0.40
0.53
0.66
0.75
1.00
1.26
1.93
SLR (m)
Existing Condition
Strategy 1 (Increased Beach Width)
Strategy 2 (Increased Beach Elevation and Width)
Land Cover Change around Lake/Pond

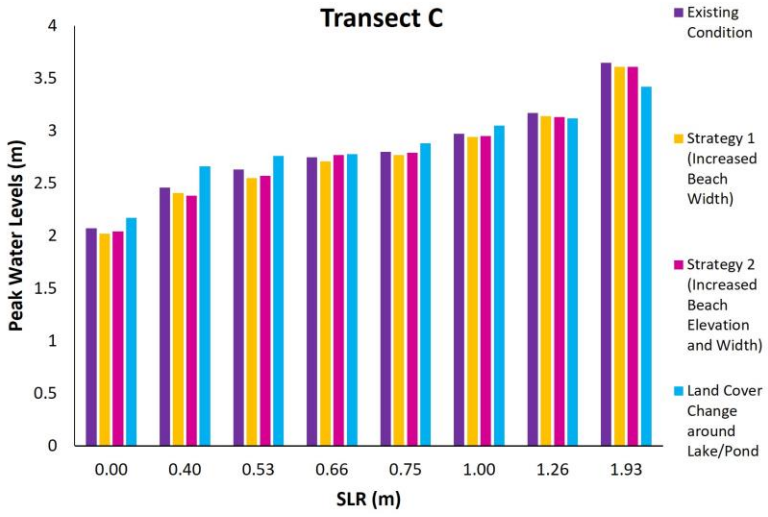
Transect C
Peak Water Levels (m)
0
0.5
1
1.5
2
2.5
3
3.5
4
0.00
0.40
0.53
0.66
0.75
1.00
1.26
1.93
SLR (m)
Existing Condition
Strategy 1 (Increased Beach Width)
Strategy 2 (Increased Beach Elevation and Width)
Land Cover Change around Lake/Pond

Final dune crest elevations from XBeach outputs were plotted with SLR scenarios (1.00, 1.26, and 1.93 m) for existing condition, Strategy 1, Strategy 2, and land cover change around Alligator Lake and Oleander Pond (Figure 21). Other SLR scenarios were not plotted since no overtopping occurred. The plots were used to determine adaptation strategy effectiveness. From Transect A, final dune crest elevations remained the same (6.05 m) at 1.00 m, 1.26 m, and 1.93 m of SLR for all adaptation strategies and land cover change. From Transect B, final dune crest elevations remained the same (4.14 m) at 1.00 m and 1.26 m of SLR. At 1.93 m of SLR, existing condition adaptation strategy yielded the lowest final dune crest elevation at 3.65 m. From Transect C, land cover change around Alligator Lake and Oleander Pond yielded the lowest final dune crest elevation at 2.34 m.

Figure 21. Final dune crest elevations were plotted with SLR for existing condition (purple bar), Strategy 1 (gold bar), Strategy 2 (pink bar), and land cover change around Alligator Lake and Oleander Pond (blue bar) for Transects A, B, and C. The horizontal black line indicates the initial dune crest elevation. Note that land cover change around Alligator Lake and Oleander Pond is not an adaptation strategy.

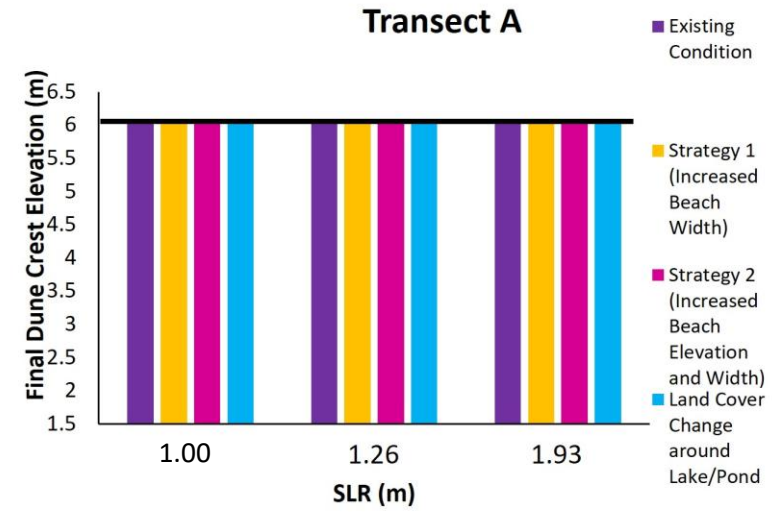
Transect A
Existing Condition
Strategy 1 (Increased Beach Width)
Strategy 2 (Increased Beach Elevation and Width)
Land Cover Change around Lake/Pond
Final Dune Crest Elevation (m)
6.5
6
5.5
5
4.5
4
3.5
3
2.5
2
1.5
1.00
1.26
1.93
SLR (m)

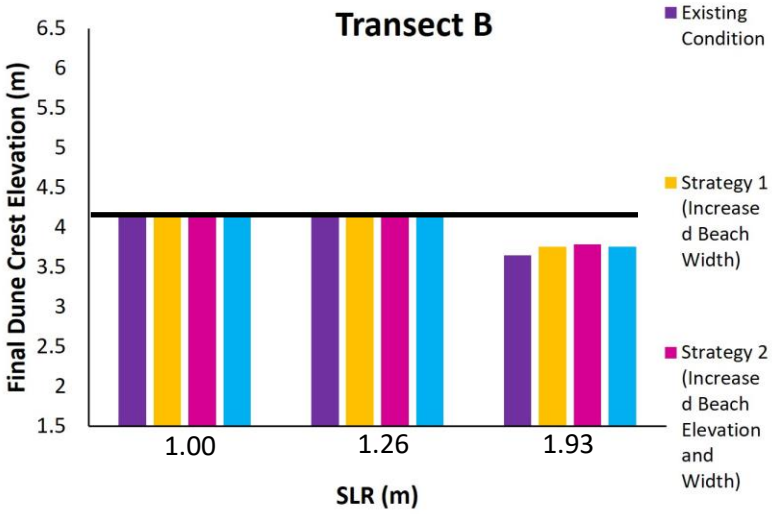
Transect B
Existing Condition
Strategy 1 (Increased Beach Width)
Strategy 2 (Increased Beach Elevation and Width)
Final Dune Crest Elevation (m)
6.5
6
5.5
5
4.5
4
3.5
3
2.5
2
1.5
1.00
1.26
1.93
SLR (m)

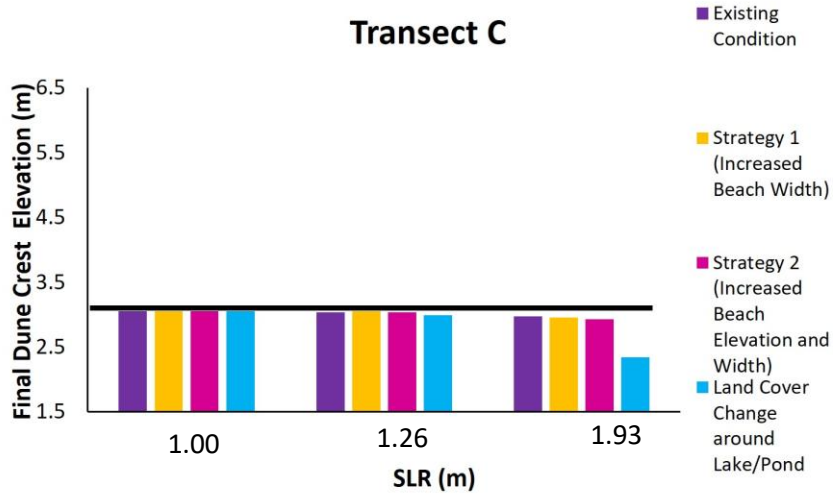
Transect C
Existing Condition
Strategy 1 (Increased Beach Width)
Strategy 2 (Increased Beach Elevation and Width)
Land Cover Change around Lake/Pond
Final Dune Crest Elevation (m)
6.5
5.5
4.5
3.5
2.5
1.5
1.00
1.26
1.93
SLR (m)

CHAPTER V

DISCUSSION

5.1 Island impacts

No SLR yielded deposition in the nearshore zone for Alligator Lake and Oleander Pond (the study site) for the existing condition, Strategy 1, Strategy 2, and land cover change around Alligator Lake and Oleander Pond. Posey (2021) also found that deposition occurred in the nearshore zone at 0.53 m of SLR for the borrow pits (developed West end) of Dauphin Island. This suggests that similar sediment transport mechanisms occurred at the East and West end of Dauphin Island on the Gulf of Mexico side. At 0.66 m of SLR, the study site did not yield dune overtopping or dune crest erosion while Posey (2021) observed total dune destruction. SLR of 1.26 and 1.93 m yielded dune overtopping at Oleander Pond for the existing condition, Strategy 1, and Strategy 2, thus resulting in contamination to the pond while Posey (2021) observed washover deposits on the back barrier side for the developed west end at 1.26 and 1.93 m of SLR. Overtopping occurred at Oleander Pond because total water levels exceeded dune crest elevations. Although island overwash on the back barrier side did not occur on the east end compared to the west end, it can be inferred that the east and west ends will likely be impacted at 1.26 m of SLR or greater through saltwater contamination and overwash, respectively. The east end cannot be completely compared to the work that Posey (2021) conducted since water levels were not simulated on the back barrier side of east end although back barrier water levels were simulated for the west end. Wave runup

likely differed between the east and west end because of different elevations on the island and differences in swash or set up.

5.2 Adaptation strategies

Discussion of adaptation strategies in this section is only described for Transect C (east side of Oleander Pond) since this location has the lowest dune elevations and experienced the most overtopping. At 1.00 m of SLR, Strategy 1 and existing condition did not yield overtopping, and the final dune crest elevations were 3.05 m. At 1.26 m of SLR, Strategy 1 and existing condition yielded overtopping, and the final dune crest elevations were 3.05 and 3.04 m. At 1.93 m of SLR, Strategy 1 and existing condition yielded overtopping, and final dune crest elevations were 2.96 and 2.97 m. The greater extent of erosion and deposition from Strategy 1 compared to existing condition is likely a result of larger sediment volume available for transport. Perhaps, the additional sand from Strategy 1 was transported to the existing beach increasing the erosion and depositional extent. The deposition at the north end of Oleander Pond is likely sediment deposited from the tributary.

At 1.00 m of SLR, Strategy 2, Strategy 1, and existing condition did not yield any overtopping, and the final dune crest elevations were 3.05 m. At 1.26 m of SLR, Strategy 2, Strategy 1, and existing condition yielded overtopping, and the final dune crest elevations were 3.04, 3.04, and 3.05 m. At 1.93 m of SLR, Strategy 2, Strategy 1, and existing condition yielded overtopping, and the final dune crest elevations were 2.93, 2.96, and 2.97 m. The greater extent of erosion and deposition from Strategy 2 compared

to Strategy 1 may have resulted from larger sediment volume available for transport. The deposition at the north end of Oleander Pond is likely sediment deposited from the tributary.

5.3 Land cover change around Alligator Lake and Oleander Pond

Land cover change around Alligator Lake and Oleander Pond was not an adaptation strategy in this study, but loss of vegetation was simulated to determine the potential impacts that could occur to the lake and pond. Although land cover change around Alligator Lake and Oleander Pond and existing condition adaptation strategies yielded the same changes in bathymetry for transect C (east side of Oleander Pond), land cover change around Alligator Lake and Oleander Pond resulted in the lowest final dune crest elevations. This indicates that the vegetation surrounding the lake, pond, and the dune systems trap sediment which is similar to Fernandez-Montblanc et al. (2020) who found that vegetation hindered overwash and sediment deposits behind the dunes. Therefore, this suggests that vegetation does lessen storm impacts and could be simulated as another adaptation strategy by vegetating the berms and dunes at the study site or other areas on the island.

5.4 Adaptation pathway

Transect C (east side of Oleander Pond) was considered in developing the adaptation pathway since the dunes at this location were most vulnerable to overtopping. At no SLR, Strategy 1 resulted in less erosion in front of the east side of Oleander Pond

than existing condition and Strategy 2. At 1.0 m of SLR, no adaptation strategies resulted in erosion of the dune crests or overtopping. Smallegan et al. (2017) suggest that routine beach nourishment for Bay Head, NJ is effective at 0.2 m of SLR. At 1.26 m of SLR, overtopping occurred for all adaptation strategies, but Strategy 1 did not result in erosion of the dune crest. At 1.93 m of SLR, all adaptation strategies resulted in overtopping and similar final dune crest elevations. Smallegan et al. (2017) found that among existing condition, routine beach nourishment, and beach and dune nourishment of a barrier island in Bay Head, NJ, beach and dune nourishment produced the least amount of maximum vertical erosion at 1.0 m and 2.2 m of SLR. Pre and post storm island volumes were not calculated in this study but would better quantify how much erosion is occurring at the dunes. Smallegan et al. (2017) simulated nourishment on the back barrier side of the island. Adaptation strategy effectiveness depends on the objectives defined and can differ based on the nature of a study site. This study focused on evaluating adaptation strategy effectiveness against overtopping and overwash rather than breaching.

Simulating storm water levels and SLR were used to determine when ATPs were reached and if alternate adaptation strategies were needed. An AP was then constructed with SLR as the *x*-axis and adaptation strategies as the *y*-axis. The adaptation pathway was constructed with respect to transect C (east side of Oleander Pond) since this area had the lowest dune elevations and was most at risk of overtopping (Figure 22). However, the adaptation pathway is representative for both Alligator Lake and Oleander Pond. No adaptation strategy is activated from 0 to 1 m of SLR, and an ATP is reached for SLR exceeding 1 m. Strategy 1 (increase beach width) is skipped and Strategy 2 (increase beach elevation and increase beach width) is activated from 1 to 2 m of SLR,

and an ATP is reached for SLR exceeding 2 m. At 2 m of SLR or greater, Strategy 3 (raise dune and beach elevations; increase beach width) is activated although it was not simulated in this study. This AP is aimed to further engage and inform stakeholders. Including this AP in a risk management plan may aid policy makers in decision making for the east end of Dauphin Island. However, further study such as simulating the adaptation strategies with additional storms and island evolution to SLR is needed to make recommendations as to which adaptation would be the most effective against a certain amount of SLR.

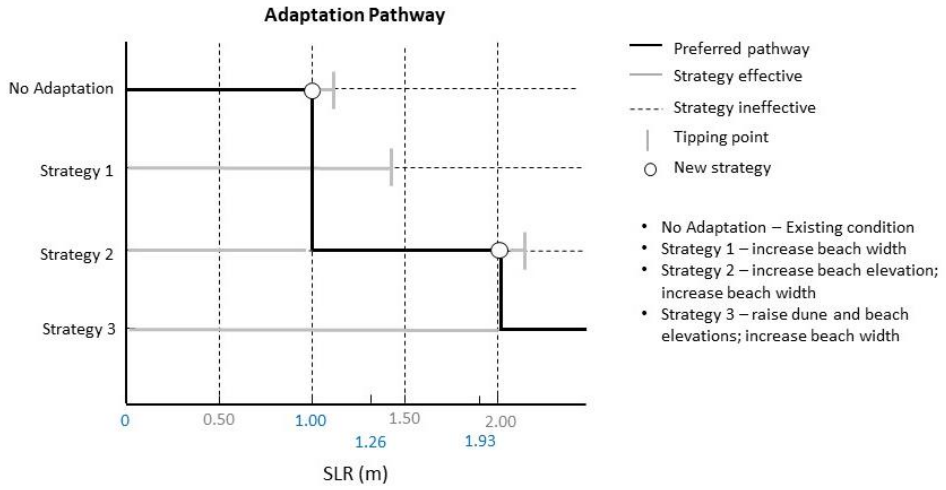

Figure 22. Adaptation strategies were plotted with respect to 0.00, 1.00, 1.26, and 1.93 m of SLR. SLR values in gray were not simulated but shown as a demonstration. Note that Strategy 3 was not simulated in this study.

Limitations to the AP are that the adaptation strategies were simulated with a numerical model XBeach which could introduce uncertainties with boundary conditions, parameters, and governing equations (Rutten et al., 2021). Uncertainties could introduce risk or hazard to computational outputs. The model used in this study was calibrated for west end because of lack of data for the east end. Only one storm (Hurricane Nate) was used in this study; other storms would potentially yield different results because of wave heights, tides, and storm surge. The superposition of SLR scenarios onto Hurricane Nate water levels is likely inaccurate since they do not interact linearly creating a bathtub approach. The bathtub approach assumes that each SLR scenario is no different than storm surge, thus simulating a storm with elevated water levels. The cross-shore profiles simulated in this study were assumed constant with SLR. However, this does not represent existing condition which continuously nourishes the beach profile as it evolves with SLR. Pre and post storm island volumes were not calculated for the study site but would give better estimates of sediment transport and thus adaptation strategy effectiveness. XBeach was not coupled with a subsurface model so the extent of groundwater contamination is unknown. The volume of seawater caused by overtopping in Oleander Pond was not calculated but would determine if remediation strategies needed to be implemented. Cost estimates were not included in this pathway which is necessary for stakeholder decision making. This AP was created for the east end of Dauphin Island which has different elevations and beach width compared to the west end of Dauphin Island. Therefore, this adaptation pathway may not apply to the same extent for other areas of Dauphin Island or other barrier islands.

Future work for this adaptation pathway could include a cost-benefit analysis, sensitivity analysis using data for the east end, validation of results, and island volume calculations, calculating seawater volume from overtopping in Oleander Pond, and coupling XBeach with a subsurface model.

CHAPTER VI

CONCLUSION

Limitations to this study such as using a bathtub approach and assuming constant cross-shore bathymetry with SLR hinder the accuracy of the results. From the three transects (A, B, and C), dune crest elevations were the lowest at Transect C (east side of Oleander Pond), causing it to be the most vulnerable to saltwater intrusion. Overtopping occurred at 1.26 and 1.93 m of SLR for existing condition, Strategy 1, Strategy 2, and land cover change around Alligator Lake and Oleander Pond for Transect C. At 1.26 m of SLR, Strategy 1 yielded the lowest dune crest erosion while existing condition yielded the lowest dune crest erosion at 1.93 m SLR. An adaptation pathway was created for Alligator Lake and Oleander Pond incorporating three simulated adaptation strategies (existing condition, Strategy 1, and Strategy 2) and one non-simulated adaptation strategy (Strategy 3).

REFERENCES

Beets, D.J. and van der Spek, A.J.F., (2000). The Holocene evolution of the barrier and the back-barrier basins of Belgium and the Netherlands as a function of late Weichselian morphology, relative sea-level rise and sediment supply, Netherlands *J. Geosci*., 79, 3 16, https://doi.org/10.1017/S0016774600021533.

Bertin, X., de Bakker, A., van Dongeren, A., Coco, G., Andrée, G., Ardhuinf, F., Bonneton, P., Bouchette, F., Castelle, B., Crawford, W., Davidson, M., Deen, M., Dodet, G., Guerin, T., Inch, K., Leckler, F., McCall, R., Muller, H., et al., and Tissier, M. (2018). Infragravity wave: From driving mechanisms to impacts. *Earth Sci. Rev*. *177*, 774-799. https://doi.org/10.1016/j.earscirev.2018.01.002

Bijlsma, L., Ehler, C.N., Klein, R.J.T., Kulshrestha, S.M., McLean, R.F., Mimura, N., Nicholls, R.J., Nurse, L.A., Perez Nieto, H., Stakhiv, E.Z., Turner, R.K., and Warrick, R.A., (1996). Coastal zones and small islands, in R.T., Watson, M.C., Zinyowera, and R.H., Moss (eds), Climate Change 1995-Impacts, Adaptations and Mitigation of *Clim Change*: Scientific-Technical Analyses, Contribution of Working Group II to the Second Assessment Report of the Intergovernmental Panel on Climate Change, Cambridge University Press, Cambridge, 289-324.

Burton, I., (1997). Vulnerability and adaptive response in the context of climate change, *Clim Change* 36 (1-2), 185-196.

Byrnes, M.R., S.F. Griffee, and M.S. Osler. (2010). Channel dredging on geomorphic response at and adjacent to Mobile Pass, Alabama, ERDC/CHL-TR-10-8, U.S.

Army Engineer Research and Development Center, Coastal and Hydraulics Laboratory, Vicksburg, MS, 309 p

Byrnes, M.R., Rosati, J.D., Griffee, S.F., Berlinghoff, J.L. (2013). Historical Sediment Transport Pathways and Quantities for Determining an Operational Sediment Budget: Mississippi Sound Barrier Islands. *J. Coast. Res.*, 63, 166-183.

Caldwell, J. (1996). Dauphin Island Water and Sewer Report.

Carruthers, E.A., Lane, D.P., Evans, R.L., Donnelly, J.P., and Ashton, A.D. (2013). Massachusetts, USA, *Mar. Geol*., 343, 15–28, https://doi.org/10.1016/j.margeo.2013.05.013

Chandler, R.V., and Moore, J.D., (1983). Fresh ground-water resources of the Dauphin Island area, Alabama: Geological Survey of Alabama Circular 109, 89 p.

Chang, S.W., Prabhakar Clement, T., Simpson, M.J., and Lee, K.K., (2011). Does Sea-level Rise Have an Impact on Saltwater Intrusion? *Adv. in Water Resour*, 1-37.

Ciarletta, D.J., Lorenza-Trueba, J., and Ashton, A.D. (2019). Mechanism for retreating barriers to autogenically form periodic deposits on continental shelves. *Geology*, 47(3), 239-242. https://doi-org.libproxy.usouthal.edu/10.1130/G45519.1

Doberstein, B., Fitzgibbons, J., and Mitchell, C. (2019). Protect, accommodate, retreat or avoid (PARA): Canadian community options for flood disaster risk reduction and flood resilience. *Nat Hazards* 98, 31–50. https://doi.org/10.1007/s11069-018-3529-z

Donnelly, C., Kraus, N., and Larson, M. (2006). State of Knowledge on Measurement and Modeling of Coastal Overwash, *J. Coast. Res.*, 22, 965–991, https://doi.org/10.2112/04-0431.1.

Donoghue, J.F. (2011). Sea level history of the northern Gulf of Mexico coast and sea level rise scenarios for the near future. *Clim Change*, 18-33.

Duran, O., and Moore, L.J. (2013). Vegetation controls on the maximum size of coastal dunes. Proc. Natl. Acad. Sci. U.S.A. 110, 17217-17222.

Ellis, A.M., Smith, C.G., and Marot, M.E. (2018). The sedimentological characteristics and geochronology of the marshes of Dauphin Island, Alabama: U.S. Geological Survey Open-File Report 2017–1165, https://doi.org/10.3133/ofr20171165

Elsayed, S.M. (2017). Breaching of Coastal Barrier under Extreme Storm Surges and Implications for Groundwater Contamination. Dissertation, 1-171.

Fernandez-Montblanc, T., Duo, E., and Ciavola, P., (2020). Dune reconstruction and revegetation as a potential measure to decrease coastal erosion and flooding under extreme storm conditions. *Ocean Coast Manag*. 188. https://doi.org/10.1016/j.ocecoaman.2019.105075

French, J.R., (2008). Hydrodynamic Modelling of Estuarine Flood Defence Realignment as an Adaptive Management Response to Sea-Level Rise. *J.Coast.Res*.24 (2B), 1–12.

Froede, C. (2008). Changes to Dauphin Island, Alabama, Brought about by Hurricane Katrina (August 29, 2005). *J.Coast.Res*. 24.4C: 110-117.

Froede, C., (2010). Constructed Sand Dunes on the Developed Barrier-Spit. *J.Coast.Res*. 699-703.

Google Earth Pro, (2021). Version 7.3.4.8248

Google Earth Pro, (2022). Version 7.3.4.8248

Guo, Weixing, and Bennett, G.D., 1998, Simulation of saline/fresh water flows using MODFLOW, in Poeter, E., and others, MODFLOW '98 Conference, Golden, Colorado, 1998, Proceedings: Golden, Colorado, v. 1, p. 267-274.

Haasnoot, M., Kwakkel, J.H., Walker, W.E., and Maat, J.T., (2013). Dynamic adaptive policy pathways: A method for crafting robust decisions for a deeply uncertain world. *Glob. Environ. Change*. 23, 485-498.

Haasnoot, M., Middlekoop, H., van Beek, E., van Deursen, W.P.A., (2011). A method to develop sustainable water management strategies for an uncertain future. *Sust. Develop*. 19, 369-381.

Haasnoot, M., Middelkoop, H., Offermans, A., van Beek, E., and van Deursen, W.P.A., (2012). Exploring pathways for sustainable water management in river deltas in a changing environment. *Clim Change*. 115, 795-819.

Haasnoot, M., Schellekens, J., Beersma, J.J., Middelkoop, H., Kwadijk, J.C.J., (2015). Transient scenarios for robust climate change adaptation illustrated for water management in The Netherlands. *Environ. Res. Lett*. 10, 105008. http://dx.doi.org/10. 1088/1748-9326/10/10/105008.

Hall, G.F., Hill, D.F., Horton, B.P., Engelhart, S.E., Peltier, W.R., (2013). A high-resolution study of tides in the Delaware Bay: Past conditions and future scenarios. *Geophys. Res. Lett*. 40, 338–342.

Halper, F.B. and W.W., Schroeder (1990). The response of shelf waters to the passage of tropical cyclones observations from the Gulf of Mexico. *Cont. Shelf Res.* 10 (8), 777-793.

Hoonhout, B., (2015). XBeach User Manual. https://xbeach.readthedocs.io/en/latest/user_manual.html

Houser, C. and Hamilton, S., (2009). Sensitivity of post-hurricane beach and dune recovery to event frequency. *Earth Surf. Process, Landf.* 34, 613-628.

IPCC, Climate Change 2007: The Physical Science Basis, Contribution of Working Group I to the Fourth Assessment Report of the Intergovernmental Panel on Climate Change, S. Solomon et al., Eds. (Cambridge Univ. Press, Cambridge, 2007).

Lazarus, E.D., (2016). Scaling laws for coastal overwash morphology, *Geophys. Res. Lett.*, 12113-12119. https://doi.org/10.1002/2016GL071213

Leatherman, S.P. (1983). Barrier dynamics and landward migration with Holocene sea-level rise, *Nature*. 301, 415-417. https://doi.org/10.1038/301415a0.

Leorri, E., Mulligan, R., Mallinson, D., Cearretta, A., (2011). Sea-level rise and local tidal range changes in coastal embayments: An added complexity in developing reliable sea-level index points. *J. Integr. Coast. Zone Manag*.11(3), 307–314.

Lorenzo-Trueba, J. and Ashton, A. D. (2014). Rollover, drowning, and discontinuous retreat: Distinct modes of barrier response to sea level rise arising from a simple morphodynamic model, *J. Geophys. Res.-Earth*. 119, 779–801, https://doi.org/10.1002/2013JF002941.

Luetrell, G.W., Hubert, M.L., Wright, W.B., Jussen, V.M., and Swanson, R.W., (1981). Lexicon of geologic names of the United States for 1968-1975: U.S. Geological Survey Bulletin 1520, p. 127.

Kanning, W., van Baars, S., van Gelder, P.H.A.J.M., and Vrijling, J.K. (2007). Lessons from New Orleans for the design and maintenance of flood defense systems. In *Risk, Reliability and Societal Safety*; Aven, T., Vinnem, J.E., Eds.; Taylor and Francis Group: London, UK

Kidd, R.E., (1988). Hydrogeology and Water-Supply Potential of the Water-Table Aquifer on Dauphin Island, Alabama. U.S. Geological Survey Scientific Investigations Report 87-4283, 1-49.

Klein, R.J.T., Nicholls, R.J., and Mimura, N., (1999). Coastal Adaptation to Climate Change: Can the IPCC technical guidelines be Applied? *Mitigation and Adaptation Strategies for Global Change*. 4, 239-252

Klein, R.J.T. and Tol, R.S.J., (1997). Adaptation to Climate Change: Options and Technologies-An Overview Paper, United Nations Framework Convention on Climate Change Secretariat, Bon, 36 pp.

Kwadijk, J.C.J., Haasnoot, M., Mulder, J.P.M., Hoogvliet, M.C., Jeuken, A.B.M., van der Krogt, R.A.A., van Oostrom, G.C., Shelfhout, H.A., van Velzen, E.H., and van Waveren, H., de Wit, M.J.M., (2010). Using adaptation tipping points to prepare for climate change and sea level rise: a case study in the Netherlands. Wiley Interdisciplinary Reviews: *Clim Change*. 1, 729-740.

MATLAB (2019). Version R2019a

Mellett, C. L. and Plater, A. J. (2018). Drowned Barriers as Archives of Coastal-Response to Sea-Level Rise, in Barrier Dynamics and Response to Changing Climate, Springer International Publishing, Cham, 57–89.

Miselis, J. L., & Lorenzo-Trueba, J. (2017). Natural and human-induced variability in barrier-island response to sea level rise. *Geophys. Res. Lett*. 44, 1, 922–931.https://doi-org.libproxy.usouthal.edu/10.1002/2017GL074811

Moore, L.J., J. H., List, S.J., Williams, and D. Stolper, (2010). Complexities in barrier island response to sea level rise: Insights from numerical experiments, North Carolina Outer Banks, *J. Geophys. Res.*, 115, F03004, doi: 10.1029/2009JF001299.

Morton, R.A. (2002). Factors controlling storm impacts on coastal barriers and beaches- a preliminary basis for near real-time forecasting. J. Coast. Res. 18, 486-501.

Morton, R.A. (2008). Historical changes in the Mississippi-Alabama barrier island chain and the roles of extreme storms, sea level, and human activities, *J. Coast. Res*. 1587-1600.

National Oceanic Atmospheric Association-Tides & Currents [NOAA-TC]. (2021). Products. Sea Level Trends. Relative Sea Level Trend. 8735180 Dauphin Island, Alabama. https://tidesandcurrents.noaa.gov/sltrends/sltrends_station.shtml?id=8735180

National Oceanic Atmospheric Association-Tides & Currents [NOAA-TC]. (2022a). Products. Sea Level Trends. Average Seasonal Cycle. 8735180 Dauphin Island, Alabama. https://tidesandcurrents.noaa.gov/sltrends/sltrends_station.shtml?id=8735180

National Oceanic Atmospheric Association-Tides & Currents [NOAA-TC]. (2022b). Products. Datums.

https://tidesandcurrents.noaa.gov/datums.html?datum=NAVD88&units=1&epoch=0&id=8735180&name=Dauphin+Island&state=AL

National Oceanic and Atmospheric Administration-National Data Buoy Center [NOAA-NDBC], (2017). Station 42012 https://www.ndbc.noaa.gov/station_history.php?station=42012

National Oceanic and Atmospheric Administration-Tides & Currents [NOAA-TC]. (2017). Products. Water Levels. Station 8735180 Dauphin Island, AL. https://tidesandcurrents.noaa.gov/waterlevels.html?id=8735180&units=standard&bdate=20170913&edate=20171013&timezone=GMT&datum=MLLW&interval=6&action=data

Nienhuis, J.H. and Lorenzo-Trueba, J. (2019). Simulating barrier island response to sea level rise with the barrier island and inlet environment (BRIE) model v1.0.

Nott, J. (2006). Tropical cyclones and the evolution of the sedimentary coast of northern Australia. *J. Coast. Res*. 22, 49–62.

OCM Partners (2022a). 2016 USACE NCMP Topobathy Lidar DEM: Gulf Coast (AL, FL, MS, TX) from 2010-06-15 to 2010-08-15. NOAA National Centers for Environmental Information, https://www.fisheries.noaa.gov/inport/item/49427.

OCM Partners (2022b). 2016 USACE NCMP Topobathy Lidar: Gulf Coast (AL, FL, MS, TX) from 2010-06-15 to 2010-08-15. NOAA National Centers for Environmental Information, https://www.fisheries.noaa.gov/inport/item/49738.

O'Donnell, D. (2005). Baseline Assessment Report 2005 for Dauphin Island Water and Sewer Authority's Public Water Supply Wells.

Otvos, E.G., Jr. (1970). Development and migration of barrier islands, northern Gulf of Mexico: Geological Society of America Bulletin, v. 81, no. 1, p. 241–246, https://doi.org/10.1130/0016-7606(1970)81[241:DAMOBI]2.0.CO;2.

Otvos, E.G., (1985). Barrier platforms: Northern Gulf of Mexico. *Mar Geol.* 63, 285-305.

Parker, D. W., E. H., Brown, and Mallory, J. C. (1981). Hurricane Frederic post-disaster report: 30 August-14 September 1979. Mobile, Alabama: US Army Corps of Engineers, Mobile District. 312. P.

Parson, E. A. & Karwat, D., (2011). Sequential climate change policy. WIRES *Clim. Change*. 2, 744-756.

Passeri, D. L., Long, J. W., Plant, N. G., Bilskie, M. V., and Hagen, S. C. (2018). The influence of bed friction variability due to land cover on storm-driven barrier island morphodynamics. *Coat Eng. 132*, 82-94. https://doi.org/10.1016/j.coastaleng.2017.11.005

Petty, K.S., (2011). The Effects of Land Cover, Climate, and Urbanization on Groundwater Resources in Dauphin Island, thesis. 1-116.

Posey, S.P., (2021). Hurricane Impacts on a Barrier Island Under Sea Level Rise Scenarios Using a Calibrated Numerical Model, thesis. 1-76.

Ramm, T. D., Watson, C. S., and White, C. J. (2018). Strategic adaptation pathway planning to manage sea-level rise and changing coastal flood risk. *Environ Sci Policy. 87*, 92-101. https://doi.org/10.1016/j.envsci.2018.06.001

Ranger, N., Reeder, T. & Lowe, J., (2013). Addressing `deep' uncertainty over long-term climate in major infrastructure projects: Four innovations of the Thames Estuary 2100 Project. EURO *J. Decis. Process*. 1**,** 233-262.

Riggs, S.R., Cleary, W.J., and Snyder, S.W., (1995). Influence of inherited geologic framework on barrier shoreface morphology and dynamics: *Mar. Geol*, v. 126, nos. 1–4, p. 213–234, https://doi.org/10.1016/0025-3227(95)00079-E.

Rodriguez, A. B., Fassell, M. L., and Anderson, J. B. (2001). Variations in shoreface progradation and ravinement along the Texas coast, Gulf of Mexico, *Sedimentology*. 48, 837–853, https://doi.org/10.1046/j.1365-3091.2001.00390.x.

Rogers, L.J., Moore, L.J., Goldstein, E.B., Hein, C.J., Lorenzo-Trueba, J., and Ashton, A.D., (2015). Anthropogenic controls on overwash deposition: Evidence and consequences, *J. Geophys. Res. Earth*. 120, 2609-2624, https://doi.org/10.1002/2015JF003634.

Rutten, J., Torres-Freyermuth, and Puleo, J. A., (2021). Uncertainty in runup predictions on natural beaches using XBeach nonhydrostatic. Coast. Eng. 166, 1-12. https://doi.org/10.1016/j.coastaleng.2021.103869

Sallenger, A. H., (2000). Storm impact scale for barrier islands. *J. Coast. Res.* 890–895.

Smallegan, S. M., Irish, J. L., and van Dongeren, A. R. (2017). Developed barrier island adaptation strategies to hurricane forcing under rising sea levels. *Clim Change*. *143*, 173-184. https://doi.org/10.1007/s10584-017-1988-y

Smit, B. (ed.), (1993). Adaptation to Climatic Variability and Change, Report of the Task Force on Climate Adaptation, Occasional Paper No. 19, University of Guelph, Guelf, 53 pp.

Smit, B., Burton, I., Klein, R.J.T., and Wandel, J., (1999). The anatomy of adaptation to climate change and variability, *Clim Change*.

Steyer, G.D., Meyers, M.B., and Spear, K.A., (2020). Alabama Barrier Island Restoration Assessment. Monitoring and Adaptive Management Plan.

Stockdon, H. F., Holman, R. A., Howd, P. A., and Sallenger, A. H. (2006). Empirical parameterization of setup, swash, and runup. *Coast. Eng. 53*, 573-588. https://doi.org/10.1016/j.coastaleng.2005.12.005

Sweet, W.V., Kopp, R.E., Weaver, C.P., Obeysekera, J., Horton, R.M., Thieler, R.E., Zervas, C. (2017). Global and Regional Sea Level Rise Scenarios for the United States. NOAA Technical Report NOS CO-OPS 083.1-56. https://doi.org/10.7289/V5/TR-NOS-COOPS-083

Thieler, E.R. and Young, R.S., (1991). Quantitative evaluation of coastal geomorphological changes in South Carolina and Hurricane Hugo. *J. Coast. Res.* 8, 187-200.

Town of Dauphin Island. (2022a). D.I. Projects. DI East End Beach and Dune Restoration. https://www.townofdauphinisland.org/_files/ugd/222868_7f9890a5e9714538bd852c49d97c7761.pdf

Town of Dauphin Island. (2022b). D.I. Projects. West End Project. https://www.townofdauphinisland.org/_files/ugd/222868_15df6311255849d58ea7ef4321f21797.pdf

Tyler, K. (2015) Sea level rise adaptation primer: a toolkit to build adaptive capacity on Canada's Coasts. Presentation. Climate Action Secretariat, BC Ministry of Environment: Prince George. http://slideplayer.com/slide/8946965/

United States Army Corps of Engineers- Engineer Research & Development Center [USACE-ERDC], (2014a). Gulf of Mexico WIS Station 73151. Annual 2014. Wind Rose. http://wis.usace.army.mil/data/gom/wdrs/ST73151_WIND_2014_01_12.png

United States. Army Corps of Engineers- Engineer Research & Development Center [USACE-ERDC], (2014b). Gulf of Mexico WIS Station 73151. Annual 2014. Wave Rose. http://wis.usace.army.mil/data/gom/wvrs/ST73151_WAVE_2014_01_12.png

United States Geological Survey [USGS], (2021). Artificial Groundwater Recharge. https://www.usgs.gov/mission-areas/water-resources/science/artificial-groundwater-recharge?qt-science_center_objects=0#qt-science_center_objects

Valentim, J.M., Vaz, L., Vaz, N., Silva, H., Duarte, B., Cacador, I., Dias, J., (2013). Sea level rise impact in residual circulation in Tagus estuary and Ria de Aveiro lagoon. *J. Coast. Res.* (SI65),1981–1986.

Vorogushyn, S., Merz, B., and Apel, H. (2009). Development of dike fragility curves for piping and micro-instability breach mechanisms. *Nat. Hazards Earth Syst. Sci.* 9, 1383-1401.

Walker, W.E., Haasnoot, M. & Kwakkel, J. H., (2013). Adapt or perish: A review of planning approaches for adaptation under deep uncertainty. *Sustainability*. 5, 955-979.

Webb, B.M., Douglass, S.L., Dixon, C.R., Buhring, B. (2011). Application of Coastal Engineering Principles in Response to the Deepwater Horizon Disaster: Lessons Learned in Coastal Alabama. *Coastal Engineering Practice*. 359-372.

Winstanley, H.C., (2013). Landsat TM-Based Analysis of Land Area and Vegetation Cover Change on Six Selected Alabama and Mississippi Barrier Islands (1984-2011). Thesis. 1-112.

Wise, R.M., Fazey, I., Smith, S.M., Park, S.E., Eakin, H.C., Archer Van Garderen, E.R.M., and Campbell, B., (2014). Reconceptualising adaptation to climate change as part of pathways of change and responses. *Glob. Environ. Change* http://dx.doi.org/10.1016/j.gloenvcha.2013.12.002

Yang, J., Graf, T., Herold, M., and Ptak, T. (2013). "Modelling the effects of tides and storm surges on coastal aquifers using a coupled surface–subsurface approach." *J. Contam Hydrol.* 149, 61–75.

Yohe, G.W., (1990). Imbedding Dynamic Responses with Imperfect Information into Static Portraits of the Regional Impact of Climate Change. Presented at International Workshop on the Natural Resource and Economic Implications of Global Climate Change, Interlaken, Switzerland, 5-9 November 1990.

BIOGRAPHICAL SKETCH

Name of Author: Kaylyn C. Bellais

Graduate and Undergraduate Schools Attended:

University of South Alabama, Mobile, Alabama

Degrees Awarded:

Master of Science in Civil Engineering, 2022, Mobile, Alabama

Bachelor of Science in Geology, 2018, Mobile, Alabama

Publications:

Smallegan, S., Collini, R., Vederal, S., Posey, P., Bellais, K., and Delaney, B. (2021). Informing and Preparing Coastal Communities to Reduce Coastal Vulnerability to Flooding and Sea-Level Rise through Education and Application: Abstract # 366099 presented at 2021 Geological Society of America Connects, October 10th-13th, Portland, OR

Bellais, K., Smallegan, S.M., and Collini, R. (2021). Adaptation Strategies to Mitigate Impacts of Sea Level Rise on a Freshwater Aquifer Supply on a Barrier Island: Abstract presented at 2021 American Shore and Beach Preservation Association Conference, September 28th-October 1st, New Orleans, LA